SUPPORTING INFORMATION

High-Yield Synthesis of Heavy Rare Earth(III) Anhydrous Solvates: Known, New, and Unexpected Products

Guilherme A. Barbosa,[a] José Severiano Carneiro Neto,[a] Bruno J. Stoeberl,[a] Sarita Wisbeck,[a] Siddhartha O. K. Giese,[a] Fabiano Yokaichiya,[b] Daniel da S. Costa,[b] Andersson Barison,[a] Ronny R. Ribeiro,[a] Leandro Piovan,[a] David L. Hughes,[c] Matteo Briganti,[d] Giordano Poneti,[e] Giovana G. Nunes,[a] Francielli S. Santana[a] and Jaísa F. Soares*[a]

[a] *Departamento de Química, Universidade Federal do Paraná, Centro Politécnico, Jardim das Américas, 81530-900 Curitiba-PR, Brazil*

[b] *Departamento de Física, Universidade Federal do Paraná, Centro Politécnico, Jardim das Américas, 81531-980 Curitiba-PR, Brazil*

[c] *School of Chemistry, University of East Anglia, Norwich NR4 7TJ, UK*

[d] *Dipartimento di Chimica "Ugo Schiff", Università degli Studi di Firenze, Via della Lastruccia 3-13, 50019 Sesto Fiorentino, Italy*

[e] *Dipartimento di Scienze Ecologiche e Biologiche, Università degli Studi della Tuscia, Largo dell'Università, 01100 Viterbo, Italy*

Summary

Scheme S1

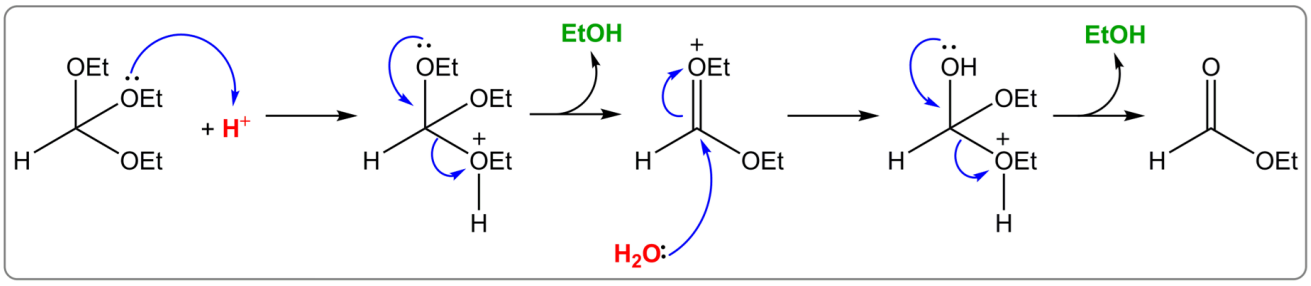

The hydrolysis of triethylorthoformate (teof) produces ethanol and ethyl formate.[1]

Single-crystal X-ray diffraction analysis (SC-XRD)

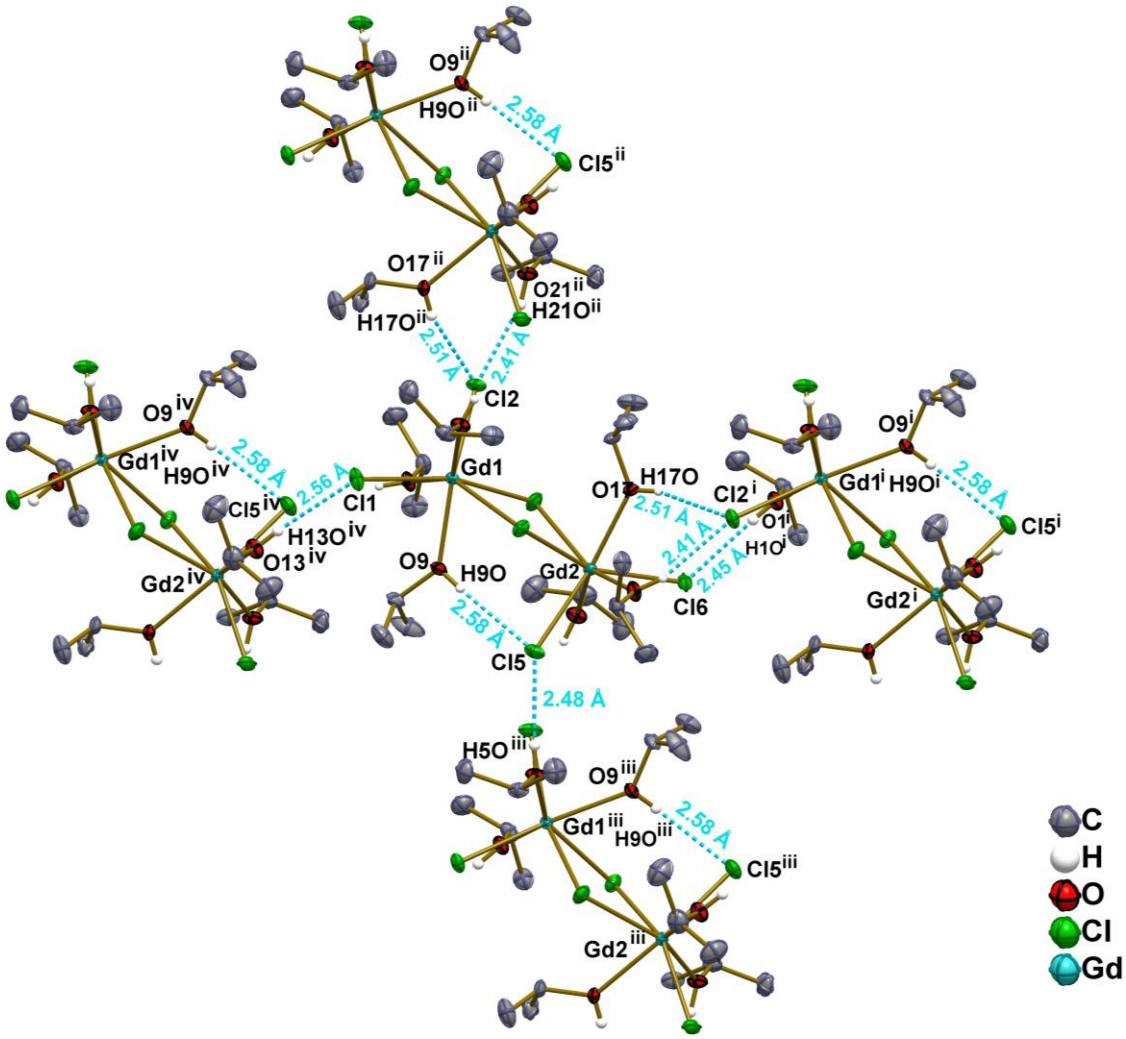

Figure S1. Representation of the intra and intermolecular hydrogen bonds in **1**, $[Gd_2Cl_4(\mu\text{–}Cl)_2(Pr^iOH)_6]$ (blue-dashed lines), with the atom numbering scheme. Hydrogen atoms were omitted for clarity, except those forming the hydroxyl groups. Thermal ellipsoids were drawn at 50% probability. Symmetry codes: (i) –x+2, y+1/2, –z+1/2, (ii) –x+2, y–1/2, –z+1/2, (iii) –x+1, y+1/2, –z+1/2, (iv) –x+1, y–1/2, –z+1/2.

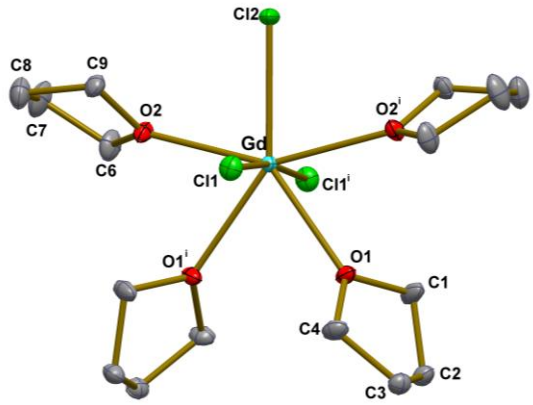

(**3**)

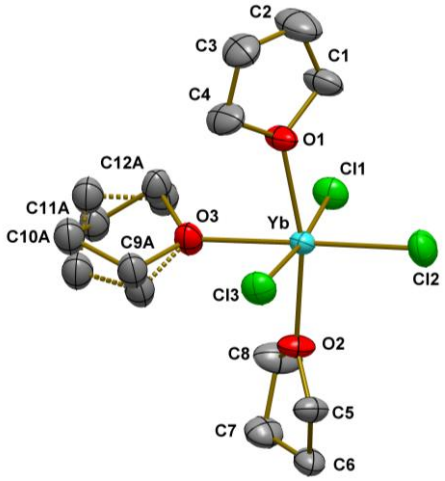

(**8**)

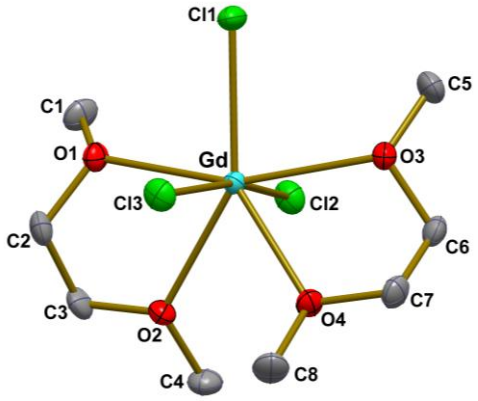

(**5**)

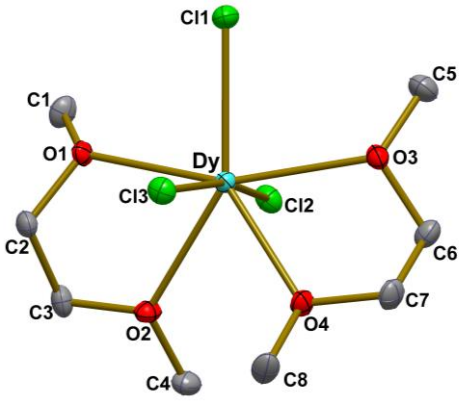

(**9**)

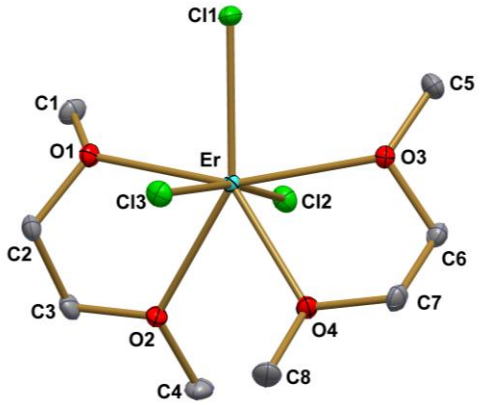

(**10**)

Figure S2. Structural representation of mononuclear products $[GdCl_3(thf)_4]$ (**3**), $[GdCl_3(dme)_2]$ (**5**), $[YbCl_3(thf)_3]$ (**8**), $[DyCl_3(dme)_2]$ (**9**), and $[ErCl_3(dme)_2]$ (**10**), with the atom numbering scheme. In **8**, the dotted bonds indicate positional disorder in the thf ligand. The ellipsoids were drawn at 50% probability, except for **8**, for which the probability level was set to 30%. These complexes were obtained by dehydration of the corresponding $RECl_3{\cdot}nH_2O$ in thf as described in the main text, and the SC-XRD structural analyses were performed to confirm the identity of the products. Complexes **3**,[2-4] **5**,[5, 6] **8**,[7] **9**,[8] and **10**[9] had been prepared earlier by other synthetic routes. Their crystal and molecular data correspond closely to those reported in this work, considering the different temperatures of data collection.

(4)

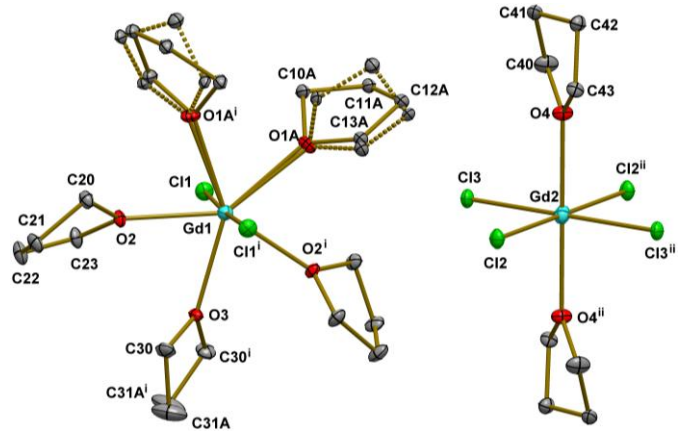

(6)

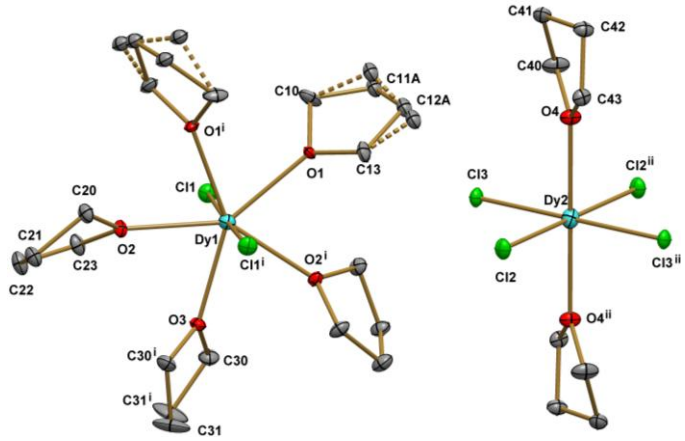

(7)

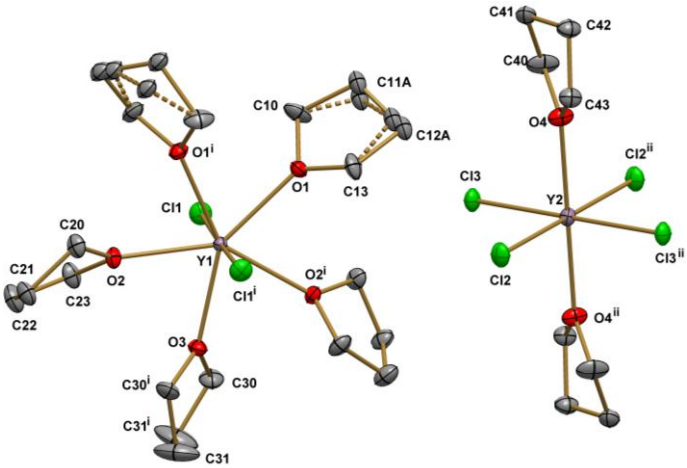

Figure S3. Structural representation of *trans*-[$MCl_2(thf)_5$]*trans*-[$MCl_4(thf)_2$], M = Gd^{3+} **(4)**, Dy^{3+} **(6)**, and Y^{3+} **(7)**, with the atom numbering scheme. The dotted bonds indicate positional disorder in the thf molecules. The ellipsoids were drawn to the 50% probability level. These complexes were obtained by dehydration of the corresponding $RECl_3{\cdot}nH_2O$ in thf as described in the main text, and the SC-XRD structural analyses were performed to confirm the identity of the products. Complexes **4**,[7, 10] **6**,[8, 11] and **7**[12] were first reported in the literature after direct reaction of the lanthanoid metal with C_2Cl_6 in thf, dehydration with thionyl chloride, and direct reaction of YCl_3 with thf under reflux (respectively). Their crystal and molecular data correspond closely to those reported in this work, considering the different temperatures of data collection.

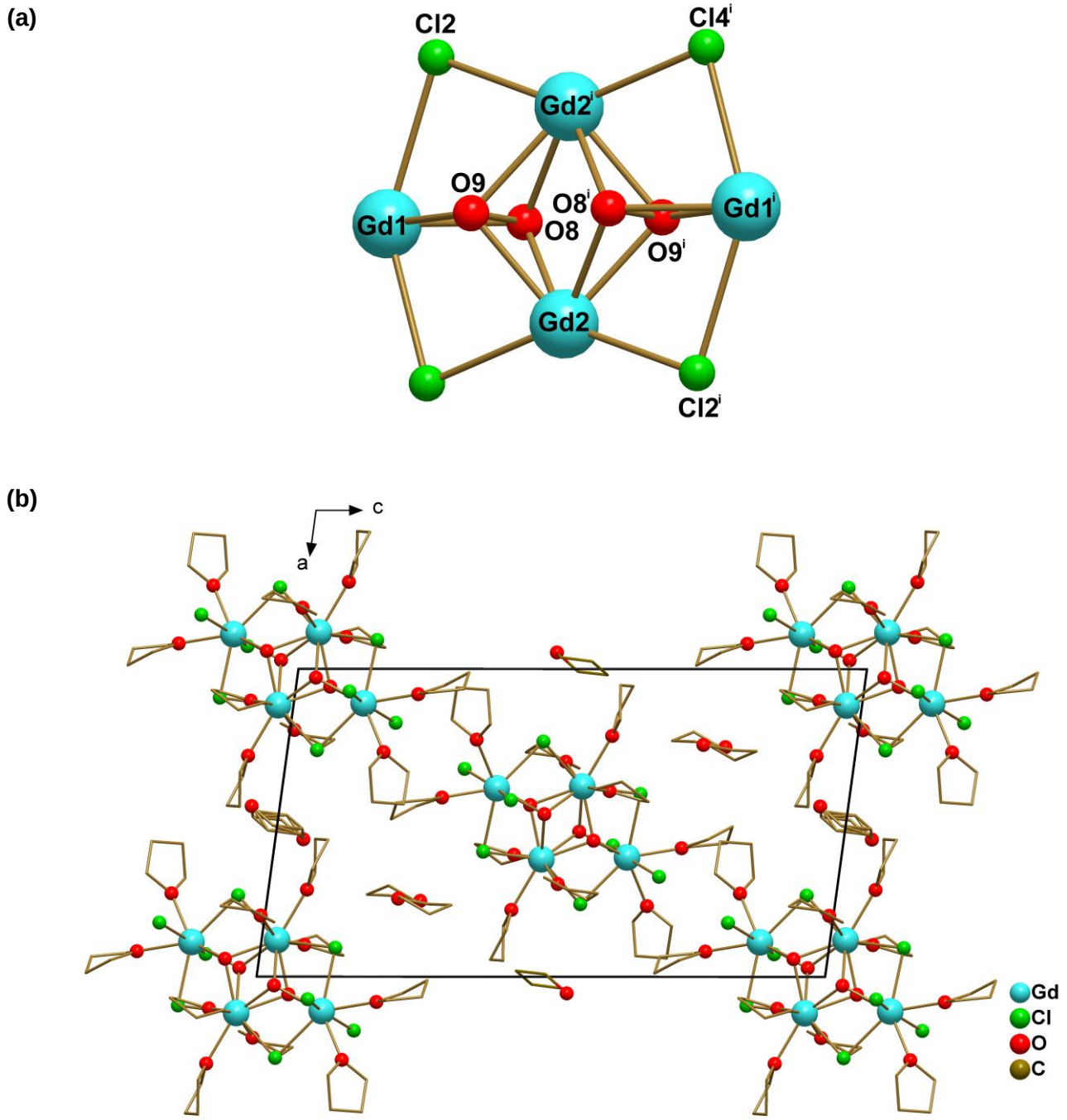

Figure S4. **(a)** Ball-and-stick model of the core structure and **(b)** packing diagram of the tetranuclear complex **12**, $[\{(thf)_2Cl_2Gd(\mu{-}Cl)_2(\mu_3{-}O_2)Gd(thf)_3\}_2]\cdot 3thf$, viewed down the *b* axis. The hydrogen atoms were omitted for clarity. Symmetry code: (i) −x+1, −y+1, −z+1.

Powder X-ray diffraction analysis (PXRD)

Due to their highly hygroscopic character and easy displacement of the coordinated ether molecules under vacuum, some of the crystalline RE-thf adducts did not provide satisfactory elemental analysis results. In these cases, PXRD analysis was instrumental in confirming the products' purity in the bulk. To minimize solvent loss, the measurements were carried out in Hilgenberg glass capillaries in which the ground crystals were sealed in contact with a small amount of the mother liquor.

Figure S5 presents the diffraction patterns registered for *trans*-[$YCl_2(thf)_5$]*trans*-[$YCl_4(thf)_2$] (**7**) and [$YbCl_3(thf)_3$] (product **8**), while Figure S6 contains an analogous plot for *trans*-[$DyCl_2(thf)_5$]*trans*-[$DyCl_4(thf)_2$] **(6)**. The experimental powder patterns match those calculated from the single-crystal data generated in this work, which are isostructural with those published previously (CCDC deposition numbers 1245798[8]/1245799[11] for **6**, 1230272[12] for **7**, and 1229954[7] for **8**).

(Figures on the next pages)

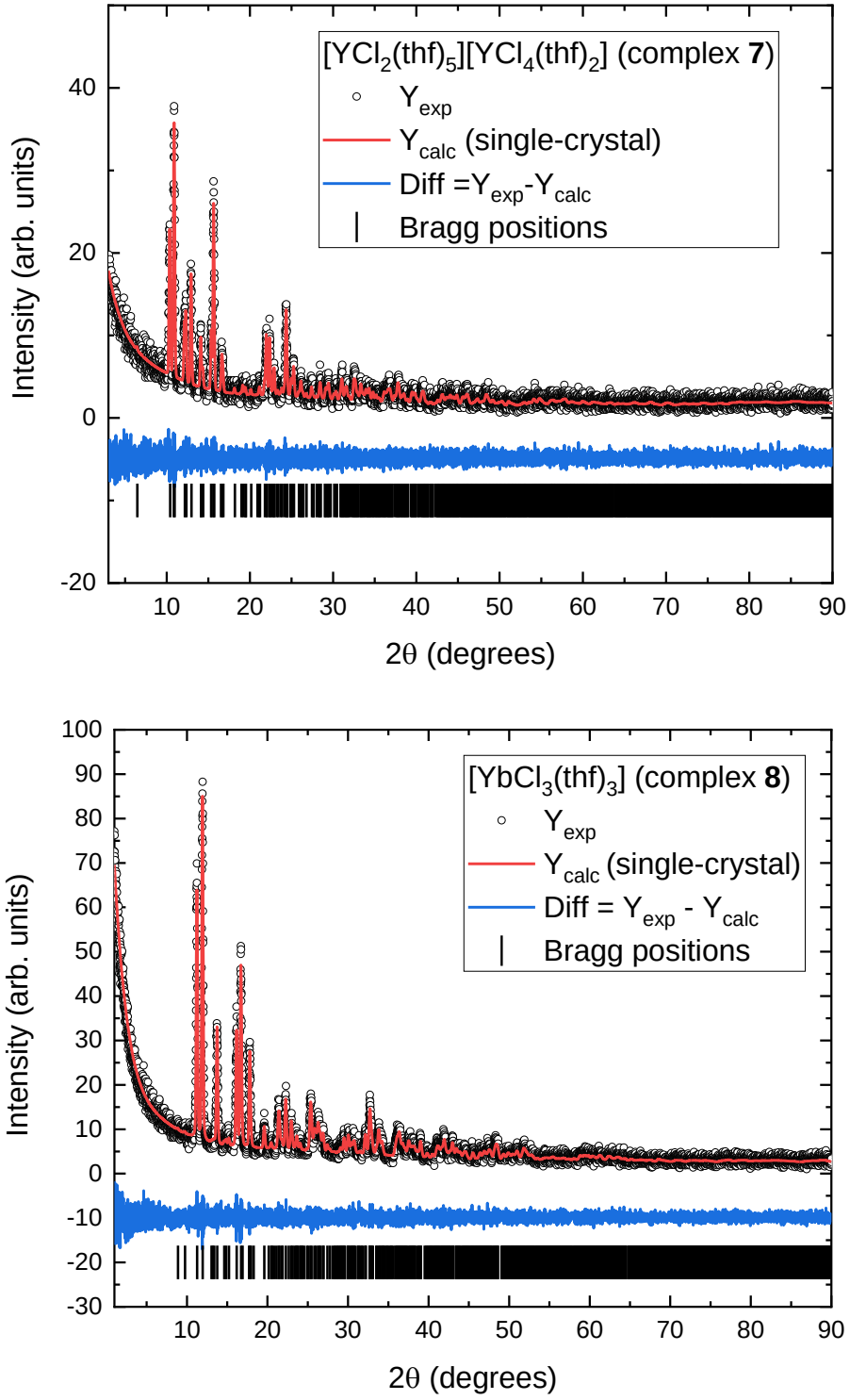

Figure S5. Calculated (red line) and experimental (black dots, Cu-Kα radiation, λ = 1.5406 Å) powder X-ray diffraction patterns for products **7,** *trans*-$[YCl_2(thf)_5]$*trans*-$[YCl_4(thf)_2]$ (top), and **8**, $[YbCl_3(thf)_3]$ (bottom). The experimental data were measured from the ground (wet) crystals sealed in Hilgenberg capillaries, as described in the Experimental (main text). No change in the crystal phase profile was observed over the measurement period of 72 h. Data refinement performed with the TOPAS software[13] confirms the presence of only one crystalline phase for each product, corresponding to those calculated from the single-crystal X-ray data (CCDC deposition numbers 2402807 (this work) and 1230272[12] for **7**, and 2402806 (this work) and 1229954[7] for **8**).

(a)

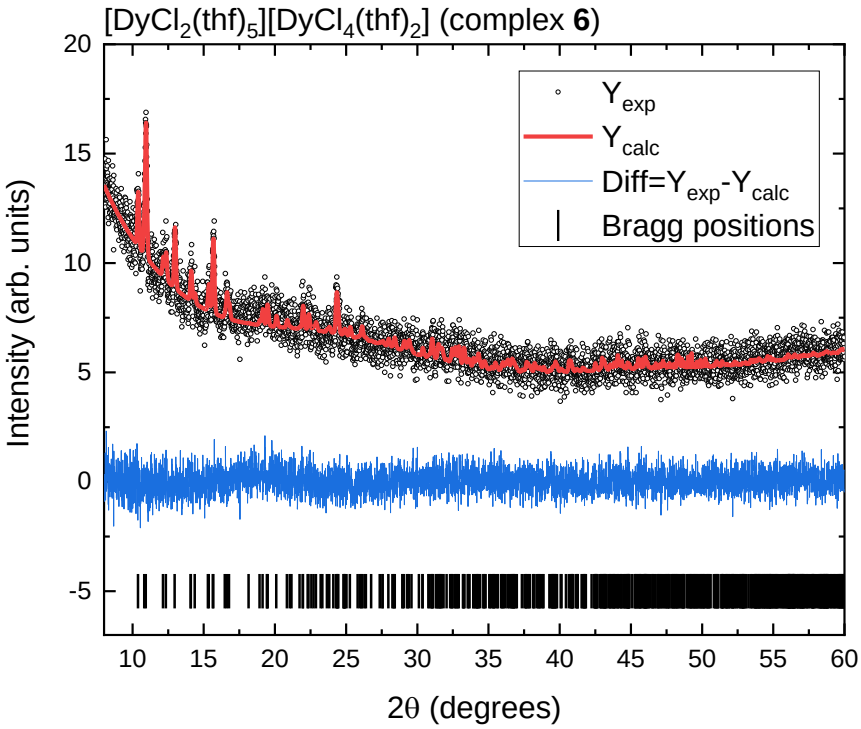

(b)

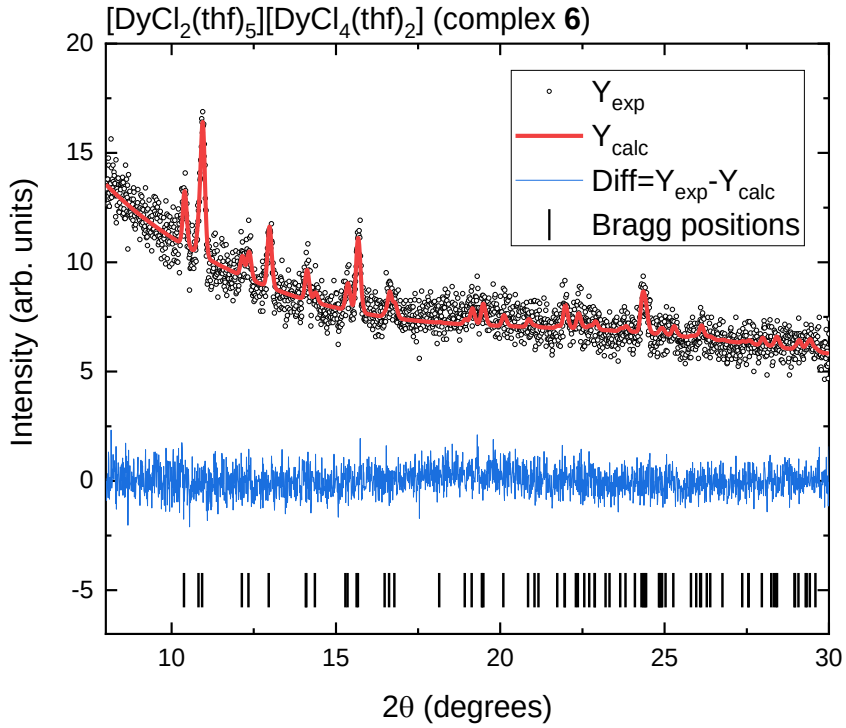

Figure S6. (a) Calculated (red line) and experimental (black dots, Cu-Kα radiation, λ = 1.5406 Å) powder X-ray diffraction patterns for the product *trans*-[$DyCl_2(thf)_5$]*trans*-[$DyCl_4(thf)_2$] **(6)**. The experimental data were measured from the ground (wet) crystals sealed in a Hilgenberg capillary. Data refinement performed with the TOPAS software[13] confirms the presence of only one crystalline phase for the product, corresponding to that calculated from the single-crystal X-ray data (CCDC deposition numbers 2402803 (this work) and 1245798[8]/1245799[11]). (b) Expansion of the 2θ = 5-30° region in Figure S6(a) for better visualization.

Infrared (FTIR) spectroscopy

The infrared spectra of all products are presented below, starting from a comparison between the new isopropanol complexes **1** and **11** (Figure S7).

Data for the remaining products (**2**-**10**, **12**) are grouped according to structural similarities, including the identity of the coordinating solvent:

- Figure S8 for the molecular thf adducts $[\{GdCl(\mu\text{–}Cl)_2(thf)_2\}s_\infty]$ (**2**), $[GdCl_3(thf)_4]$ (**3**) and $[YbCl_3(thf)_3]$ (**8**);
- Figure S9 for the discrete ion pair thf complexes *trans*-$[MCl_2(thf)_5]$*trans*-$[MCl_4(thf)_2]$, M = Gd (**4**), Dy (**6**), and Y (**7**);
- Figure S10 for the tetranuclear Gd complex **12** with peroxide and thf ligands;
- Figure S11 for the dimethoxyethane complexes $[LnCl_3(dme)_2]$, Ln = Gd (**5**), Dy (**9**), and Er (**10**).

Band assignments based on literature data[2, 5, 9, 11, 12, 14-16] and corresponding discussion follow the plots to facilitate comparison.

(Figures and discussion on the next pages)

1. Gd–isopropanol adducts **1** and **11**

In the FTIR spectrum of **1**, a high-intensity band at 3378 cm^{-1} is attributed to coordinated isopropanol's ν(O–H) stretching. This absorption appears at a lower energy in the coordination polymer **11** (3251 cm^{-1}), possibly because, in the latter, all hydroxyl groups are involved in hydrogen bonds. The Pr^{i}OH ν(C–O) and $\rho_r(CH_3)$ vibrations occur in **1** at 1088 and 930 cm^{-1}, respectively, while **11** presents more than one band assignable to each of these vibration modes (1090, 1045, 1011, 918 cm^{-1}) due to the different bond environments in the isopropanol, 2-methoxyethanol, and acetate ligands. The band at 813 cm^{-1} in **1** can be assigned to a Pr^{i}OH carbon skeleton vibration, and it again has more than one equivalent in **11** (835, 814 cm^{-1}).[15, 17]

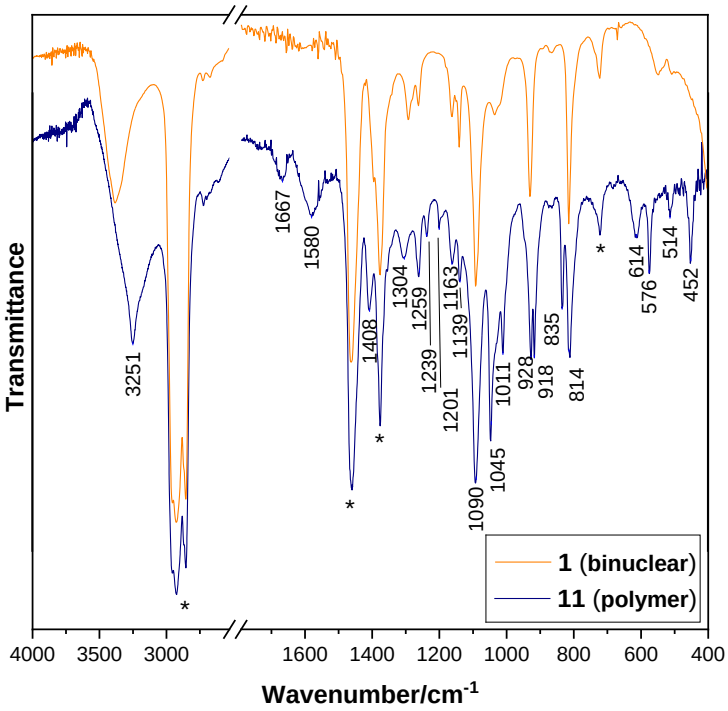

Figure S7. FTIR spectra (Nujol mull) registered for complexes **1**, [$Gd_2Cl_4(\mu\text{-}Cl)_2(Pr^iOH)_6$], and **11**, [{$Gd_3Cl_3(\mu\text{-}Cl)_4(\mu\text{-}H_3CCOO)(C_3H_8O_2)(Pr^iOH)_4]\cdot Pr^iOH\}_\infty$]. The mineral oil gives the bands marked with asterisks at 720, $\rho(CH_2)$; 1378, δ(C–H, CH_3); 1460 δ(C–H, CH_2) and 2825-2995 cm^{-1} (ν(C–H)).[18]

The acetate ligand in **11** presents typical absorptions assigned according to the literature[15, 19] (see the following table). The difference $\nu_a(COO)-\nu_s(COO)$ = 172 cm^{-1} is in excellent agreement with a bridging carboxylate group and, therefore, with the single-crystal XRD results (Figure 5, main text).

Wavenumber (cm^{-1})	Assignment[19]	Wavenumber (cm^{-1})	Assignment[19]
1580	$\nu_a(COO)$	928	ν(CC)
1408	$\nu_s(COO)$	614	π(CH) or π(COO)
1045	$\rho_r(CH_3)$	576	δ(CCO)
1011	$\rho_r(CH_3)$	452	δ(CH) or $\rho_r(COO)$

ν_a, antisymmetric stretching; ν_s, symmetric stretching; ρ_r, rocking; π, out-of-plane bending; δ, in-plane bending or deformation.[15]

2. Tetrahydrofuran adducts, molecular (**2**, **3**, and **8**) and ion pair (**4**, **6**, and **7**)

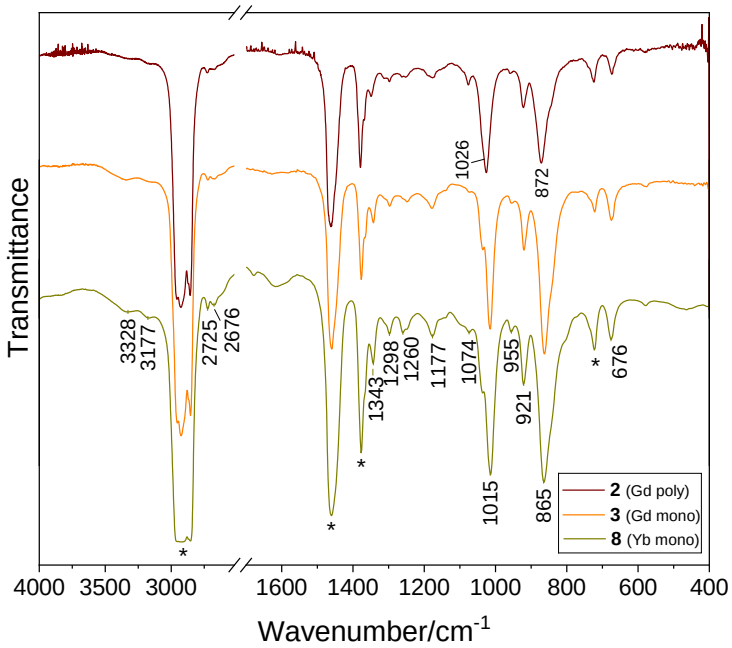

Figure S8. FTIR spectra (Nujol mulls) registered for the molecular thf adducts [{GdCl(μ–Cl)$_2$(thf)$_2$}$_\infty$] (product **2**), [GdCl$_3$(thf)$_4$] (**3**) and [YbCl$_3$(thf)$_3$] (**8**). Asterisks indicate mineral oil absorptions.

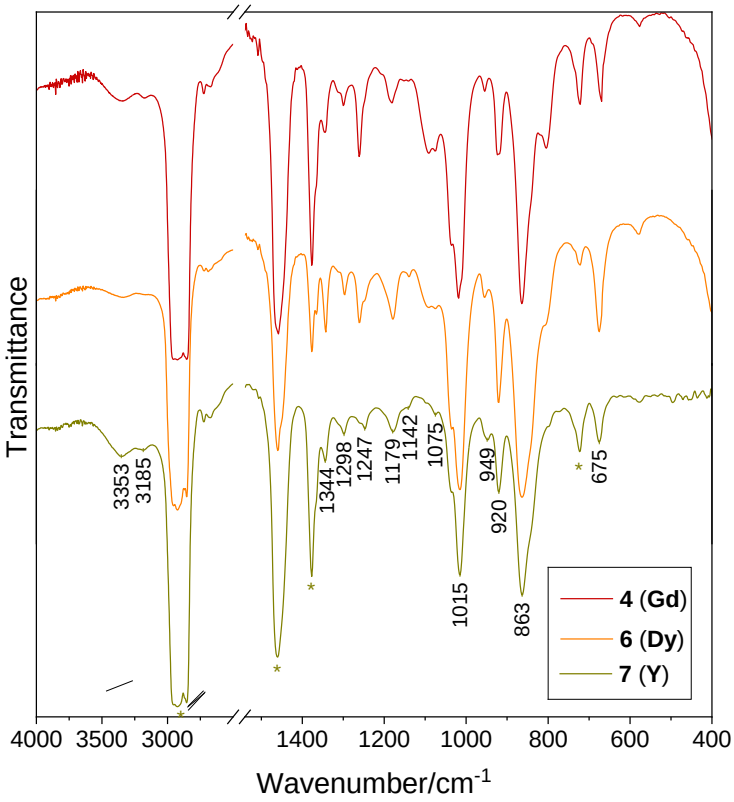

Figure S9. FTIR spectra (Nujol mulls) registered for the discrete ion pair complexes *trans*-[MCl$_2$(thf)$_5$]*trans*-[MCl$_4$(thf)$_2$], M = Gd (**4**), Dy (**6**), and Y (**7**). Asterisks indicate mineral oil absorptions.

The FTIR spectra registered for the compounds with thf as ligand are all very similar, with minor intensity variations that do not clearly distinguish between the mononuclear or polymeric, molecular or ion pair, products. This impossibility highlights the limits of the technique and the relevance of X-ray diffraction analysis in characterizing these products. The two high-intensity bands registered at *ca* 865 cm^{-1} and 1015 cm^{-1} are assigned to ν_s(C–O–C) and ν_{as}(C–O–C), respectively, confirming the presence of bound tetrahydrofuran.[2, 11, 14, 15] The other bands are typical of the thf skeletal vibrations.

3. Tetranuclear, peroxido-bridged Gd_4-thf adduct **12**, $[Gd_4(O_2)_2Cl_8(thf)_{10}]\cdot 3thf$

Figure S10 compares the FTIR spectra of the two polynuclear thf adducts **2**, $[\{GdCl(\mu\text{–}Cl)_2(thf)_2\}_\infty]$, and **12**, $[\{(thf)_2Cl_2Gd(\mu\text{-}Cl)_2(\mu_3\text{-}O_2)Gd(thf)_3\}_2]\cdot 3thf$. In **2**, the lower intensity bands at 920 and 1072 cm^{-1} could come from unbound thf, as the crystals were not extensively dried after removal from the mother liquor to avoid crystallinity loss. They contrast with the stronger bands at 872 and 1024 cm^{-1} for the coordinated ligands, also registered for the other thf adducts reported in this work (Figures S8 and S9). In the case of **12**, besides the presence of crystallizing thf in the unit cell, a few drops of the solvent were added to the crystals before grinding and mixing with Nujol, and this could explain the higher intensity of the 920 and 1072 cm^{-1} bands. Besides these absorptions, **12** presents additional strong bands at 862 and 887 cm^{-1} assigned to ν_s(C–O–C) and 1019 and 1036 cm^{-1}, ν_{as}(C–O–C), evidencing the different binding sites for thf coordinated to Gd1/Gd1' and Gd2/Gd2'. Because of the strong absorptions in the 800-950 cm^{-1} region, it is impossible to identify the usually low-to-medium intensity band assigned to the characteristic O–O stretching vibration of peroxides in **12**.[15, 20]

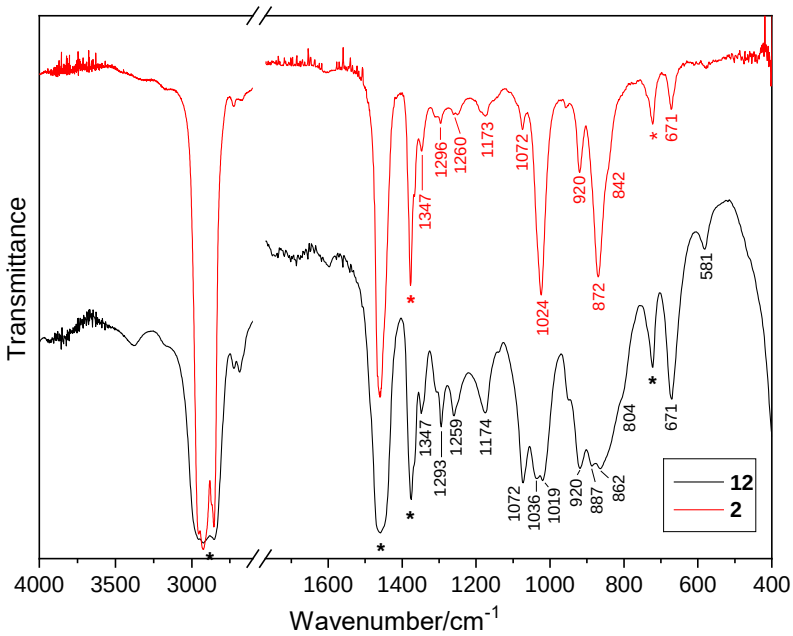

Figure S10. FTIR spectra (Nujol mulls) for the polymeric $[\{GdCl(\mu\text{–}Cl)_2(thf)_2\}_\infty]$ (product **2**) and the tetranuclear **12,** $[\{(thf)_2Cl_2Gd(\mu\text{-}Cl)_2(\mu_3\text{-}O_2)Gd(thf)_3\}_2]\cdot 3thf$. Asterisks indicate mineral oil absorptions.

4. Dimethoxyethane adducts **5**, **9**, and **10**

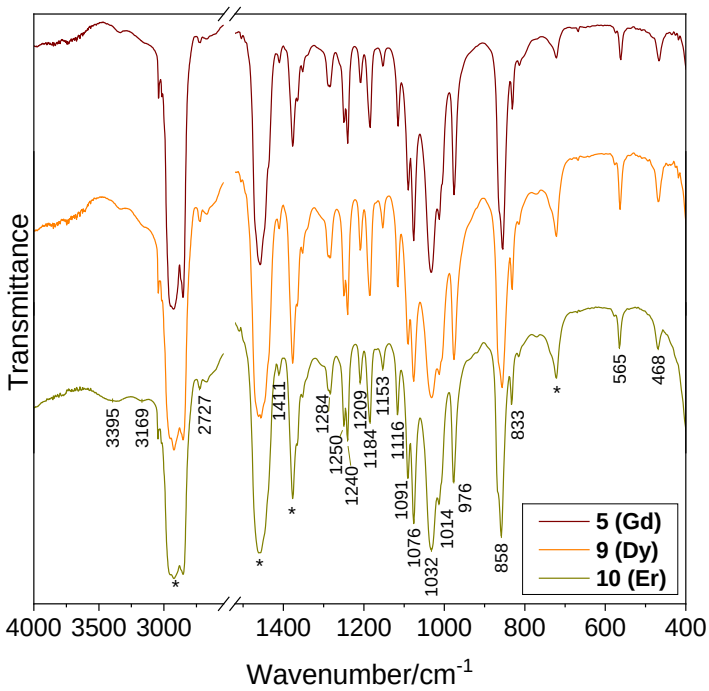

Figure S11. FTIR spectra (Nujol mulls) registered for the dimethoxyethane adducts [$LnCl_3(dme)_2$], Ln = Gd (**5**), Dy (**9**), and Er (**10**). Asterisks indicate mineral oil absorptions.

The FTIR spectra of the products with 1,2-dimethoxyethane are mainly superimposable, with well-defined and sharp bands whose intensities vary with sample concentration. The strong absorptions at *ca* 860 cm^{-1} and 1080 cm^{-1} are assigned to ν_s(C–O–C) and ν_{as}(C–O–C), respectively,[9] in addition to the bands at 1187 and 1033 cm^{-1}, $\rho_r(CH_3)$, 976 cm^{-1}, ν(C–O), and 830 cm^{-1}, $\rho(CH_3)$, all consistent with the presence of the dme ligand.[5, 16]

Magnetic susceptibility measurements for the Dy^{3+} products **6** and **9**

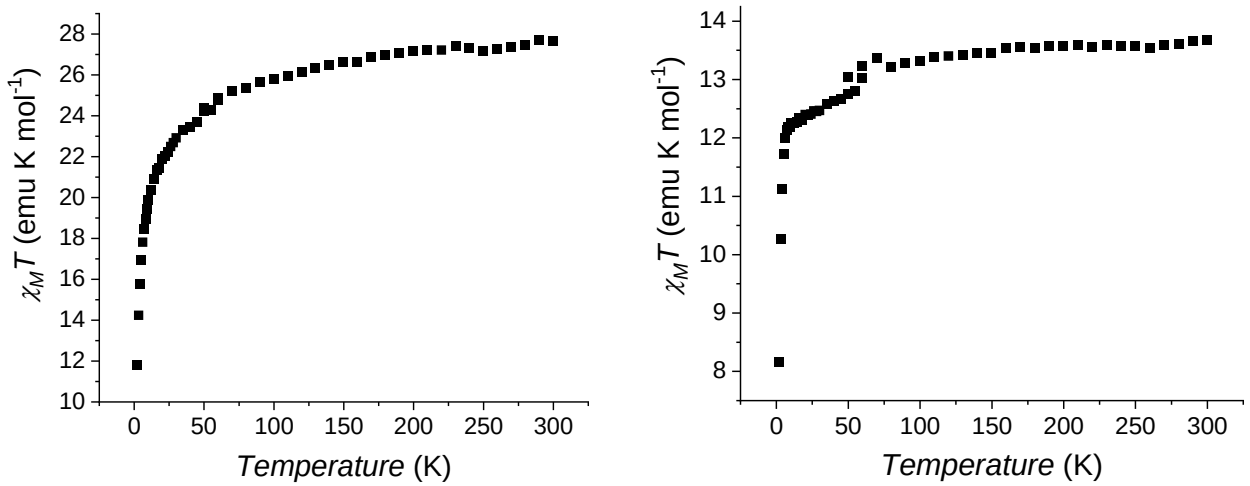

Figure S12. Dependence of $\chi_M T$ (molar magnetic susceptibility multiplied by temperature) on the temperature for products **6**, *trans*–$[DyCl_2(thf)_5]$*trans*–$[DyCl_4(thf)_2]$ (left), and **9**, $[DyCl_3(dme)_2]$ (right).

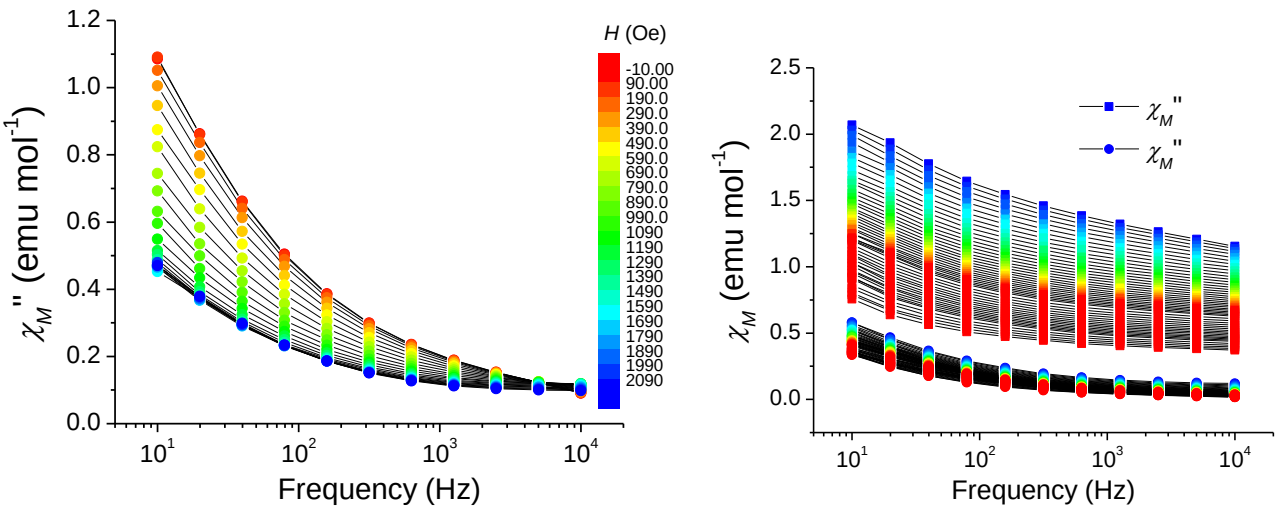

Figure S13. Left: Isothermal (T = 2.0 K) scan of the out-of-phase magnetic susceptibility for product **6** in different applied static fields (0-2 kOe). *Right:* Temperature scan of the frequency dependence of the in- and out-of-phase magnetic susceptibilities of product **6** for a 1.0 kOe applied static field.

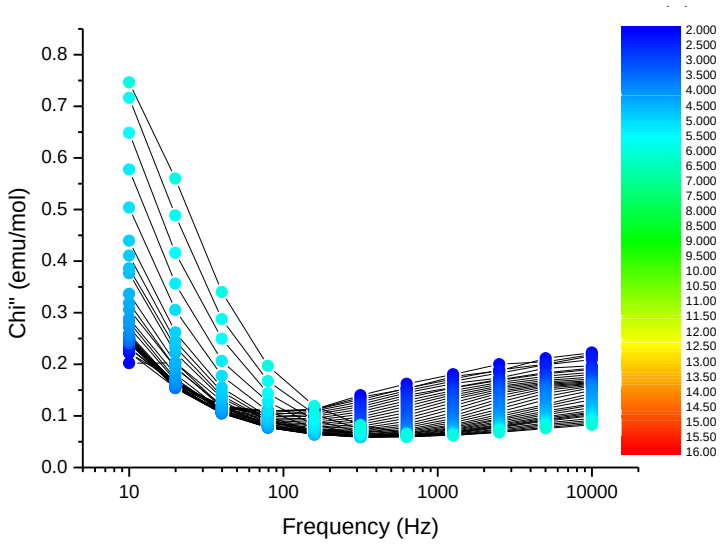

Figure S14. Extract from the $\chi''(\nu)$ plot in Figure 4 (main text) for product **9**, limited to the 1.9-6 K range, showing the high-frequency peaks. The measurements were carried out with an applied static field of 1 kOe.

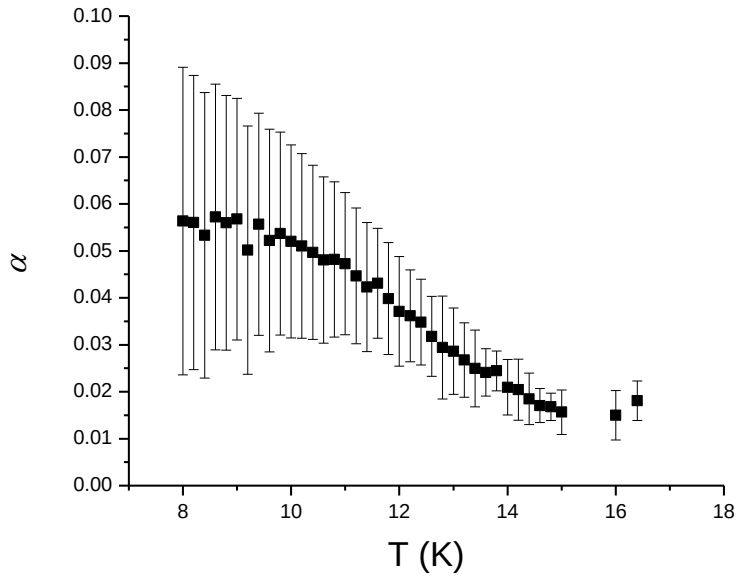

Figure S15. Temperature dependence of the statistical distribution of magnetic relaxation times (α) for the slow-relaxing component of $\chi''(\nu)$ for product **9**, $[DyCl_3(dme)_2]$.

X-band CW-EPR spectroscopy

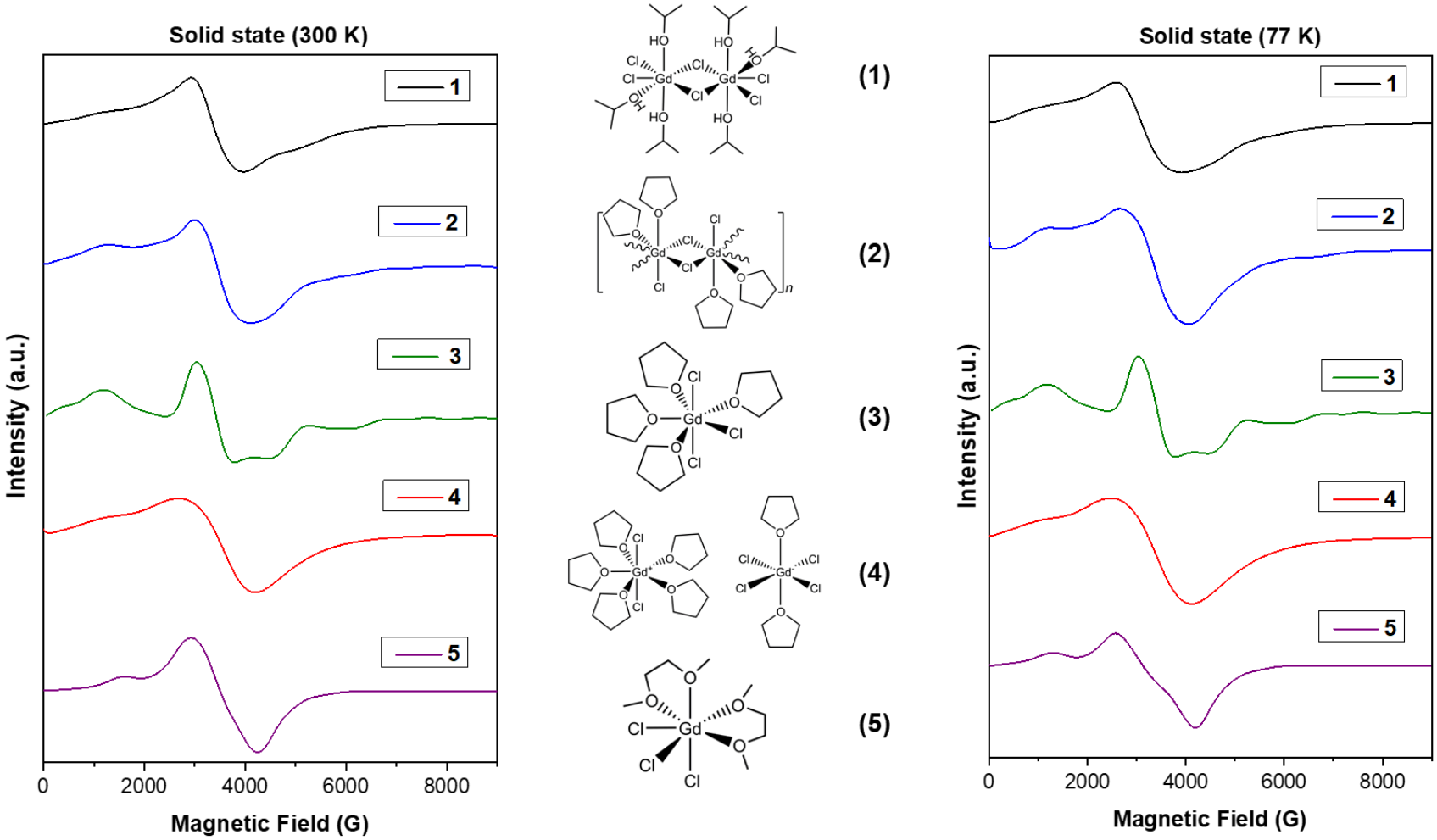

Figure S16. X-band (9.4 GHz) CW-EPR spectra registered for ground crystals of the Gd^{3+} complexes **1**-**5** at 300 K (left) and 77 K (right).

^{1}H NMR spectroscopy

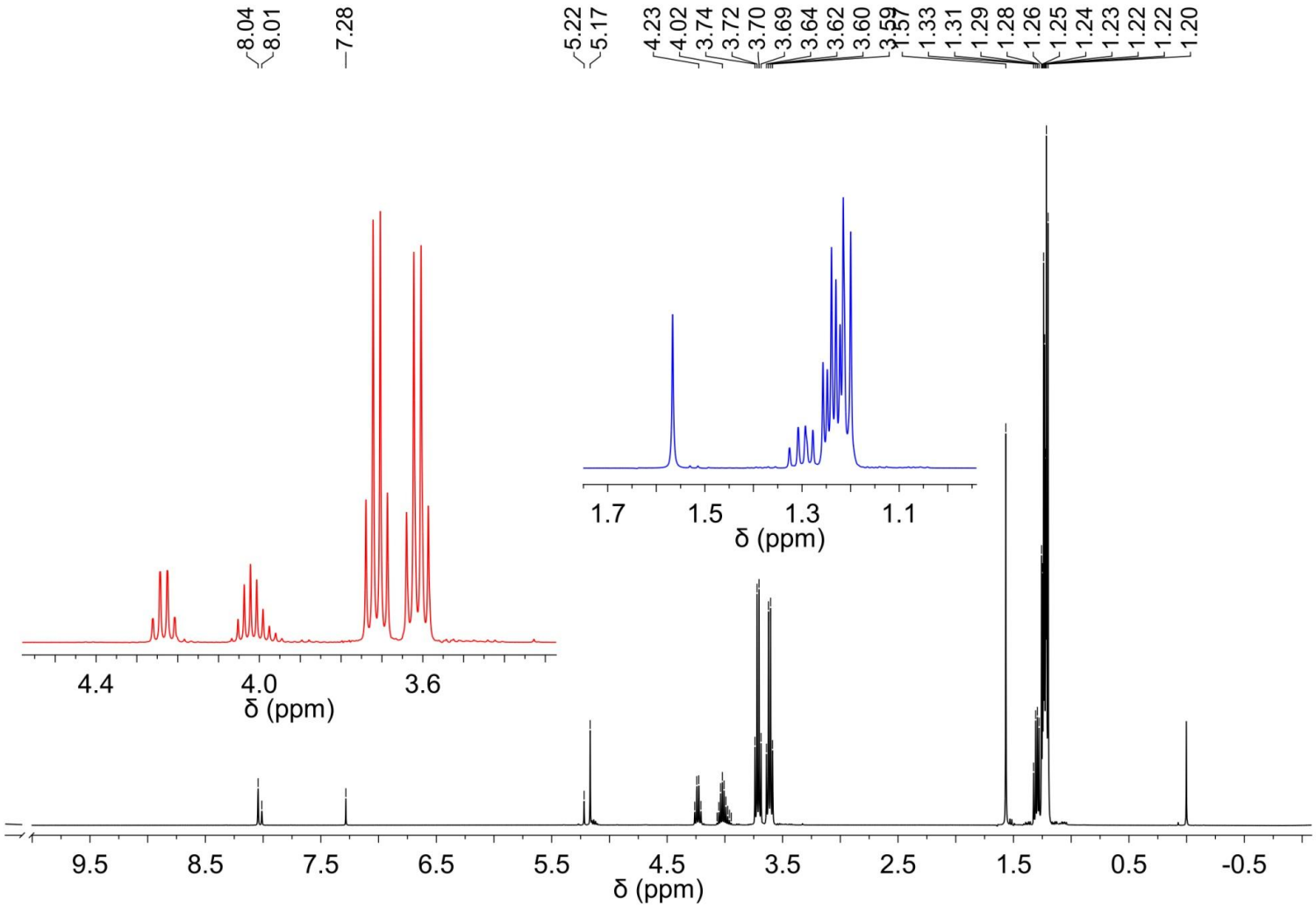

Figure S17. ^{1}H (400.13 MHz) spectra of the volatiles collected from the reaction mixture that produced the polymeric complex **11**, [{$Gd_3Cl_4(\mu–Cl)_4(\mu–H_3CCOO)(C_3H_8O_2)(Pr^iOH)_4]\cdot Pr^iOH\}_\infty$]. The volatiles were evaporated by vacuum pumping and recovered by condensation in liquid N_2 when the reaction mixture was dried to give Product **A** (see Experimental in the main text). Solvent: $CDCl_3$. Reference: tetramethylsilane (tms) at 0.00 ppm. Peak assignments are presented in Table S13.

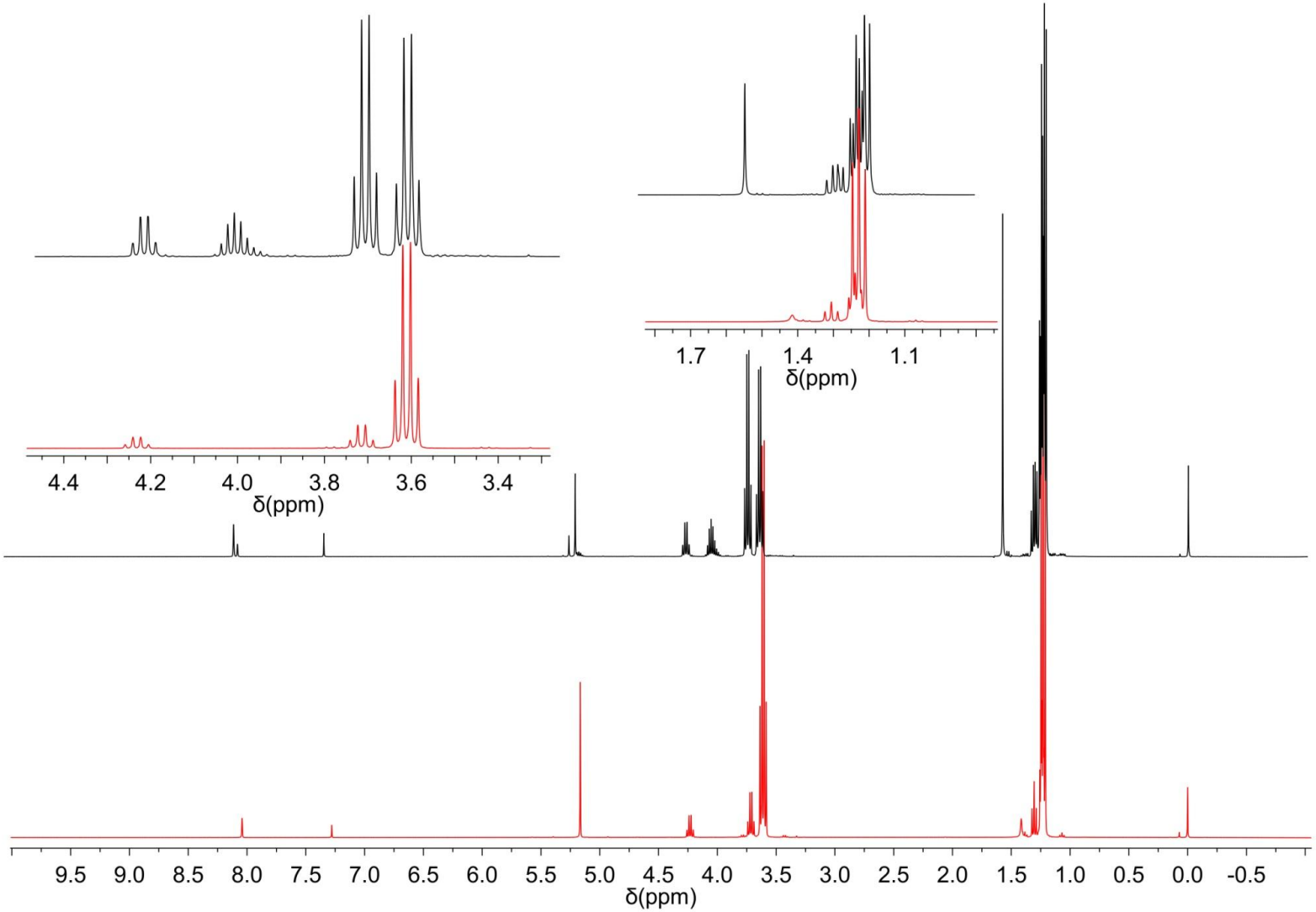

Figure S18. Comparison of the ^{1}H (400.13 MHz) spectra of *(a)* commercial trielthylorthoformate, red line, and *(b)* the volatiles collected from the reaction mixture that produced the polymeric complex **11**, $[\{Gd_3Cl_4(\mu\text{–}Cl)_4(\mu\text{–}H_3CCOO)(C_3H_8O_2)(Pr^iOH)_4]\cdot Pr^iOH\}_\infty]$ (black line). The volatiles were evaporated by vacuum pumping and recovered by condensation in liquid N_2 when the reaction mixture was dried to give Product **A** (see Experimental in the main text). Solvent: $CDCl_3$. Reference: tms at 0.00 ppm. Peak assignments are presented in Table S13.

SUPPLEMENTARY TABLES

Table S1. Crystal and refinement data for $[Gd_2(\mu–Cl)_2(Pr^iOH)_6]$ (**1**), $[\{GdCl(\mu–Cl)_2(thf)_2\}_\infty]$ (**2**), $[\{Gd_3Cl_4(\mu–Cl)_4(\mu–H_3CCOO)(C_3H_8O_2)(Pr^iOH)_4]\cdot Pr^iOH\}_\infty]$ (**11**), and $[\{(thf)_2Cl_2Gd(\mu\text{-}Cl)_2(\mu_3\text{-}O_2)Gd(thf)_3\}_2]\cdot 3thf$ (**12**). Wavelength: 0.71073 Å (Mo-K_α). Temperature of data collection: 100(2) K

Complex	(**1**)	(**2**)	(**11**)	(**12**)
Elemental formula	$C_{18}H_{48}Cl_6O_6Gd_2$ (**1**)	$C_8H_{16}Cl_3O_3Gd$ (**2**)	$C_{20}H_{51}Cl_8Gd_3O_9$ (**11**)	$C_{40}H_{80}Cl_8Gd_4O_{14}$, 3($C_4H_8O$) (**12**)
CCDC deposition number	2402796	2402799	2402797	2402798
Formula weight (g mol^{-1})	887.76	407.81	1190.95	1913.95
Crystal system / Space group	Monoclinic / $P2_1/c$	Triclinic / P–1	Triclinic / P–1	Monoclinic / $P2_1$/n
Unit cell axes (Å)	a = 11.9739(11)	a = 8.188(4)	a = 11.2739(5) Å	a = 13.2553(11)
	b = 15.0639(14)	b = 8.480(4)	b = 12.2225(5) Å	b = 10.9651(9)
	c = 18.2762(19)	c = 9.656(4)	c = 15.6040(8) Å	c = 24.264(2)
Unit cell angles (º)	$\alpha = \gamma = 90$	α = 79.66(2)	α = 81.216(2)°	
	β = 94.004(4)	β = 70.541(18)	β = 78.827(3)°	β = 97.715(4)
		γ = 82.603(19)	γ = 74.501(2)°	
Cell volume (Å^3) / Z / F(000)	3288.5(5) / 4 / 1736	620.2(5) / 2 / 390	2021.08(16) / 2 / 1142	3494.8(5) / 2 / 1888
Crystal color, shape	Colorless blocks	Colorless needles	Colorless plates	Colorless blocks
Density, calculated (Mg m^{-3})	1.793	2.184	1.957	1.819
Absorption coefficient (mm^{-1})	4.513	5.966	5.431	4.111
θ range for data collection (º)	2.9 to 27.5	2.9 to 27.5	2.9 to 27.5	3.6 to 27.5
hkl range	$-15 \le h \le 15$	$-10 \le h \le 10$	$-14 \le h \le 14$	$-17 \le h \le 17$
	$-19 \le k \le 19$	$-11 \le k \le 11$	$-15 \le k \le 15$	$-14 \le k \le 14$
	$-23 \le l \le 23$	$-12 \le l \le 12$	$-20 \le l \le 20$	$-31 \le l \le 31$
Reflections collected / unique	173673 / 7548 [R(int) = 0.036]	73150 / 2844 [R(int) = 0.046]	164401 / 9289 [$R_{(int)}$ = 0.134]	250280 / 8011 [R(int) = 0.064]
No. of 'observed' reflections (I > 2σ_I)	7217	2737	7378	7290
Absorption correction / Refinement	Multi-scan / Least squares / Full matrix in F^2	Gaussian from crystal shape Least squares / Full matrix in F^2	Multi-scan / Least squares / Full matrix in F^2	Multi-scan / Least squares / Full matrix in F^2
Transmission (max / min)	0.7457 / 0.5713	0.8327 / 0.4259	0.7461 / 0.5802	0.7461 / 0.5800
Data / restrictions / parameters	7548 / 1 / 325	2844 / 0 / 127	9289 / 1 / 397	8011 / 4 / 377
Goodness-of-fit (F^2)	1.122	1.120	1.047	1.135
Final R indexes [I>2σ(I)] *	R_1 = 0.014; wR_2 = 0.030	R_1 = 0.010; wR_2 = 0.026	R_1 = 0.032; wR_2 = 0.049	R_1 = 0.022, wR_2 = 0.048
Final R indexes (all data) *	R_1 = 0.015; wR_2 = 0.030	R_1 = 0.012; wR_2 = 0.026	R_1 = 0.053; wR_2 = 0.053	R_1 = 0.027, wR_2 = 0.049
Largest diff. peak and hole (e Å^{-3})	1.00 and –0.46	0.72 and –0.62	0.87 and –0.81	1.04 and -0.76
Location of the largest diff. peak	0.70 Å from Gd2	0.79 Å from Gd1	0.90 Å from H1O	0.92 Å from Gd1

(*) (**1**) $w = [\sigma^2(F_o^2)+(0.0115\ P)^2+2.8354\ P]^{-1}$ with $P = (F_o^2+2F_c^2)/3$
(**2**) $w = [\sigma^2(F_o^2)+(0.0153\ P)^2+0.2272\ P]^{-1}$ with $P = (F_o^2+2F_c^2)/3$
(**11**) $w = [\sigma^2(F_o^2)+(0.0042\ P)^2+8.9100\ P]^{-1}$ with $P = (F_o^2+2F_c^2)/3$
(**12**) $w = [\sigma^2(F_o^2)+(0.0156\ P)^2+9.0321\ P]^{-1}$ with $P=(F_o^2+2F_c^2)/3$

Table S2. Selected dimensions (bond distances, Å, and angles, °) involving the metal ions in complex **1**, $[Gd_2Cl_4(\mu–Cl)_2(Pr^iOH)_6]$. Standard deviations are in parentheses

Bond lengths / Å			
O1–Gd1	2.3918(12)	Cl2–Gd1	2.6782(4)
O5–Gd1	2.4064(12)	Cl3–Gd2	2.7234(4)
O9–Gd1	2.4011(13)	Cl3–Gd1	2.7822(4)
O13–Gd2	2.3832(13)	Cl4–Gd2	2.7945(4)
O17–Gd2	2.4025(13)	Cl4–Gd1	2.7662(4)
O21–Gd2	2.3695(12)	Cl5–Gd2	2.6774(5)
Cl1–Gd1	2.6295(4)	Cl6–Gd2	2.6476(4)
Angles / °			
Gd1–O1–H1O	120.0(19)	O13–Gd2–Cl6	78.29(3)
Gd2–O21–H21O	112.8(18)	O13–Gd2–Cl3	78.05(3)
Gd2–O17–H17O	116(2)	O17–Gd2–Cl6	76.89(3)
Gd1–O5–H5O	119.2(18)	O17–Gd2–Cl5	152.54(4)
Gd1–O9–H9O	120(2)	O17–Gd2–Cl3	78.36(3)
Gd2–O13–H13O	126(2)	O17–Gd2–Cl4	78.77(3)
Gd1–Cl4–Gd2	102.485(15)	O21–Gd2–Cl4	81.81(3)
Gd2–Cl3–Gd1	103.923(15)	O21–Gd2–Cl5	82.71(3)
C2–O1–Gd1	131.38(10)	O21–Gd2–Cl6	77.77(3)
C6–O5–Gd1	131.62(10)	O21–Gd2–Cl3	150.51(3)
C10–O9–Gd1	133.86(11)	Cl1–Gd1–Cl2	109.486(15)
C14–O13–Gd2	125.18(11)	Cl1–Gd1–Cl3	155.882(13)
C18–O17–Gd2	134.15(10)	Cl1–Gd1–Cl4	116.082(15)
C22–O21–Gd2	132.79(10)	Cl2–Gd1–Cl3	79.670(14)
O1–Gd1–Cl4	74.96(3)	Cl2–Gd1–Cl4	118.590(14)
O1–Gd1–Cl3	122.76(3)	Cl3–Gd2–Cl4	75.692(14)
O1–Gd1–Cl1	81.34(3)	Cl4–Gd1–Cl3	75.214(14)
O1–Gd1–Cl2	73.62(3)	Cl5–Gd2–Cl3	110.727(14)
O5–Gd1–Cl1	78.94(3)	Cl5–Gd2–Cl4	78.662(13)
O5–Gd1–Cl2	81.34(3)	Cl6–Gd2–Cl5	118.695(14)
O5–Gd1–Cl4	144.45(3)	Cl6–Gd2–Cl3	114.479(15)
O5–Gd1–Cl3	80.58(3)	Cl6–Gd2–Cl4	150.758(13)
O9–Gd1–Cl1	82.77(4)	O1–Gd1–O5	140.59(4)
O9–Gd1–Cl2	155.02(4)	O1–Gd1–O9	130.83(5)
O9–Gd1–Cl3	81.20(4)	O9–Gd1–O5	79.82(4)
O9–Gd1–Cl4	71.12(3)	O13–Gd2–O17	134.40(5)
O13–Gd2–Cl4	130.86(3)	O21–Gd2–O13	131.44(4)
O13–Gd2–Cl5	72.91(3)	O21–Gd2–O17	78.77(4)

Table S3. Selected dimensions (bond distances and angles) about the metal ions in complex **2**, [{GdCl(μ–Cl)$_2$(thf)$_2$}$_\infty$]. Bond lengths are in Angstroms (Å) and angles in degrees (°). Standard deviations are in parentheses

Bond lengths / Å			
Gd1–O1	2.4014(14)	Gd1–Cl1^{ii}	2.7727(11)
Gd1–O2	2.4174(14)	Gd1–Cl2	2.7996(9)
Gd1–Cl3	2.5791(11)	Gd1–Cl1^{ii}	2.7727(11)
Gd1–Cl1	2.7401(10)	Gd1–Cl2^{i}	2.7431(11)
Gd1–Cl2^{i}	2.7431(11)		
Angles / °			
O1–Gd1–O2	94.11(5)	Cl2^{i}–Gd1–Cl1^{ii}	140.43(2)
O1–Gd1–Cl3	174.40(3)	O1–Gd1–Cl2	98.52(4)
O2–Gd1–Cl3	82.59(4)	O2–Gd1–Cl2	140.82(3)
O1–Gd1–Cl1	84.66(4)	Cl3–Gd1–Cl2	86.84(3)
O2–Gd1–Cl1	144.44(3)	Cl1–Gd1–Cl2	73.95(3)
Cl3–Gd1–Cl1	95.37(3)	Cl2^{i}–Gd1–Cl2	71.34(3)
O1–Gd1–Cl2^{i}	80.90(4)	Cl1^{ii}–Gd1–Cl2	146.385(14)
O2–Gd1–Cl2^{i}	74.33(3)	Gd1–Cl1–Gd1^{ii}	107.45(3)
Cl3–Gd1–Cl2^{i}	102.44(3)	Gd1^{i}–Cl2–Gd1	108.66(3)
Cl1–Gd1–Cl2^{i}	139.71(2)	C13–O1–Gd1	116.51(9)
O1–Gd1–Cl1^{ii}	81.12(4)	C10–O1–Gd1	135.00(10)
O2–Gd1–Cl1^{ii}	72.16(3)	C20–O2–Gd1	121.18(9)
Cl3–Gd1–Cl1^{ii}	93.54(3)	C23–O2–Gd1	125.03(9)
Cl1–Gd1–Cl1^{ii}	72.55(3)		

Symmetry code: (i) –x+1,–y,–z+1; (ii) –x+1,–y+1,–z+1.

Table S4. Crystal and refinement data for complexes $[GdCl_3(thf)_4]$ (**3**), $[GdCl_3(dme)_2]$ (**5**), $[YbCl_3(thf)_3]$ (**8**), $[DyCl_3(dme)_2]$ (**9**), and $[ErCl_3(dme)_2]$ (**10**)

Complex	**3**	**5**	**8**	**9**	**10**
Elemental formula	$C_{16}H_{32}Cl_3GdO_4$	$C_8H_{20}Cl_3GdO_4$	$C_{12}H_{24}Cl_3O_3Yb$	$C_8H_{20}Cl_3DyO_4$	$C_8H_{20}Cl_3ErO_4$
CCDC deposition number	2402801	2402802	2402806	2402804	2402805
Molar mass (g mol^{-1})	552.02	443.84	495.70	449.09	453.85
Crystal system, space group	Orthorhombic, *F*dd2	Monoclinic, $P2_1/c$	Monoclinic, $P2_1/c$	Monoclinic, $P2_1/c$	Monoclinic, $P2_1/c$
a (Å)	16.3487(9)	11.4344(8)	9.057(3)	11.3517(9)	11.2875(4)
b (Å)	29.4984(16)	8.8655(6)	12.863(4)	8.8174(7)	8.7925(4)
c (Å)	9.0581(5)	15.6127(11)	15.697(5)	15.5541(12)	15.5229(7)
Angles (°)	90, 90, 90	90, 104.808(2), 90	90, 92.150(10), 90	90, 104.726(3), 90	90; 104.5990(10); 90
Volume (Å^3)	4368.4(4)	1530.12(18)	1827.4(9)	1505.7(2)	1490.84(11)
Z	8	4	4	4	4
Density (Mg m^{-3})	1.679	1.927	1.802	1.981	2.022
Temperature (K)	100(2)	173(2)	300(2)	100(2)	100(2)
F(000)	2200	860	964	868	876
Absorption coefficient (mm^{-1})	3.419	4.854	5.557	5.491	6.163
Crystal color, shape	colorless block	colorless parallelepiped	colorless block	colorless block	Light-pink block
θ range (°)	3.7 to 27.5	2.8 to 28.3	2.2 to 27.5	2.9 to 26.7	3.6 to 28.3
Reflections collected	80788	113452	24558	94827	113869
Unique data	2488 [$R_{(int)}$ = 0.038]	3808 [$R_{(int)}$ = 0.040]	3364 [$R_{(int)}$ = 0.051]	3183 [$R_{(int)}$ = 0.051]	3673 [$R_{(int)}$ = 0.022]
Observed data, [I > 2σ(I)]	2414	3470	2399	2687	3588
Absorption correction / Refinement	Multi-scan / Least squares / Full matrix in F^2				
Data / restrictions / parameters	2488 / 1 / 110	3808 / 0 / 149	3364 / 116 / 204	3183 / 0 / 149	3673 / 0 / 149
Goodness-of-fit on F^2	1.115	1.150	1.166	1.254	1.265
R_1 [I > 2σ(I)], wR_2 [I > 2σ(I)]	0.009, 0.021	0.013, 0.027	0.043, 0.102	0.034, 0.065	0.010, 0.024
R_1, wR_2 (all data)	0.009, 0.021	0.016, 0.028	0.063, 0.113	0.053, 0.077	0.012, 0.024
Largest diff. peak and hole (e·Å^{-3})	0.49 and −0.16	0.29 and −0.51	1.66 and −1.06	3.75 and −2.53	0.48 and −0.56
Location of the largest difference peak	1.61 Å from H1A	0.73 Å from C3	2.04 Å from Cl2	1.53 Å from H6A	0.74 Å from C6

(**3**) $w = [\sigma^2(F_o^2)+(0.0118\ P)^2+0.2626\ P]^{-1}$ with $P = (F_o^2+2F_c^2)/3$
(**5**) $w = [\sigma^2(F_o^2)+(0.0129\ P)^2+0.3468\ P]^{-1}$ with $P = (F_o^2+2F_c^2)/3$
(**8**) $w = [\sigma^2(F_o^2)+(0.0311)^2+10.5920\ P]^{-1}$ with $P = (F_o^2+2F_c^2)/3$
(**9**) $w = [\sigma^2(F_o^2)+19.5865\ P]^{-1}$ with $P = (F_o^2+2F_c^2)/3$
(**10**) $w = [\sigma^2(F_o^2)+(0.0007\ P)^2+1.6425\ P]^{-1}$ with $P = (F_o^2+2F_c^2)/3$

Table S5. Crystal and refinement data for the ion pair complexes *trans*-[$GdCl_2(thf)_5$]*trans*-[$GdCl_4(thf)_2$] **(4),** *trans*-[$DyCl_2(thf)_5$]*trans*-[$DyCl_4(thf)_2$] **(6),** and *trans*-[$YCl_2(thf)_5$]*trans*-[$YCl_4(thf)_2$] **(7)**

Complex	**4**	**6**	**7**
Elemental formula	$C_{20}H_{40}Cl_2GdO_5$, $C_8H_{16}Cl_4GdO_2$	$C_{20}H_{40}Cl_2DyO_5$, $C_8H_{16}Cl_4DyO_2$	$C_{20}H_{40}Cl_2O_5Y$, $C_8H_{16}Cl_4O_2Y$
CCDC deposition number	2402800	2402803	2402807
Molar mass (g mol^{-1})	1031.92	1042.42	895.24
Crystal system, space group	Monoclinic, *C*2/c	Monoclinic, *C*2/c	Monoclinic, *C*2/c
a (Å)	12.5685(11)	12.5509(10)	12.5609(8)
b (Å)	11.4240(10)	11.3841(9)	11.3719(7)
c (Å)	26.624(2)	26.6104(18)	26.5618(18)
Angles (°)	90, 94.117(3), 90	90, 93.812(2), 90	90, 93.908(3), 90
Volume (Å^3)	3812.9(6)	3793.7(5)	3785.3(4)
Z	4	4	4
Density (Mg m^{-3})	1.798	1.825	1.571
Temperature (K)	100(2)	100(2)	100(2)
F(000)	2040	2056	1840
Absorption coefficient (mm^{-1})	3.908	4.371	3.514
Crystal color, shape	colorless block	colorless plate	colorless block
θ range (°)	3.6 to 25.6	2.9 to 25.5	2.8 to 27.5
Reflections collected	3536	108251	88936
Unique data	3536 [$R_{(int)}$ = 0.090]	3533 [$R_{(int)}$ = 0.097]	4335 [$R_{(int)}$ = 0.058]
Observed data, [I > 2σ(I)]	3146	3331	3919
Absorption correction / Refinement	Multi-scan Least squares / Full matrix in F^2	Gaussian from crystal shape Least squares / Full matrix in F^2	Multi-scan Least squares / Full matrix in F^2
Data / restrictions / parameters	3536 / 171 / 226	3533 / 7 / 198	4335 / 6 / 199
Goodness-of-fit on F^2	1.096	1.192	1.033
R_1 [I > 2σ(I)], wR_2 [I > 2σ(I)]	0.026, 0.055	0.030, 0.065	0.025, 0.051
R_1, wR_2 (all data)	0.034, 0.057	0.033, 0.066	0.031, 0.052
Largest diff. peak and hole (e·Å^{-3})	0.76 and −0.53	1.06 and −1.80	0.50 and −0.57
Location of the largest difference peak	1.34 Å from Gd1	1.07 Å from H12C	0.38 Å from C11B

(**4**) $w = [\sigma^2(F_o^2)+(0.0498\ P)^2+46.8667\ P]^{-1}$ with $P = (F_o^2+2F_c^2)/3$
(**6**) $w = [\sigma^2(F_o^2)+(0.0131\ P)^2+43.8794\ P]^{-1}$ with $P = (F_o^2+2F_c^2)/3$
(**7**) $w = [\sigma^2(F_o^2)+ (0.0171\ P)^2+9.2251\ P]^{-1}$ with $P = (F_o^2+2F_c^2)/3$

Table S6. Selected bond lengths (Å) for complexes $[GdCl_3(thf)_4]$ (**3**), $[GdCl_3(dme)_2]$ (**5**), $[YbCl_3(thf)_3]$ (**8**), $[DyCl_3(dme)_2]$ (**9**), and $[ErCl_3(dme)_2]$ (**10**), with estimated standard deviations in parentheses. Symmetry code: (i) –x+1, –y+1,z

Bond type	$[GdCl_3(thf)_4]$ (**3**)		$[GdCl_3(dme)_2]$ (**5**)		$[DyCl_3(dme)_2]$ (**9**)		$[ErCl_3(dme)_2]$ (**10**)		$[YbCl_3(thf)_3]$ (**8**)	
$Ln–O_{thf}$	Gd–O1	2.4724(13)	-----	-----	-----	-----	-----	-----	Yb–O1	2.254(5)
	Gd–O1^{i}	2.4724(13)							Yb–O2	2.277(5)
	Gd–O2	2.4221(14)							Yb–O3	2.366(6)
	Gd–O2^{i}	2.4221(14)							-----	-----
$Ln–O_{dme}$	-----	-----	Gd–O1	2.4213(11)	Dy–O1	2.401(4)	Er–O1	2.3687(11)	-----	-----
			Gd–O2	2.4960(10)	Dy–O2	2.467(4)	Er–O2	2.4467(11)		
			Gd–O3	2.4714(11)	Dy–O3	2.444(4)	Er–O3	2.4204(11)		
			Gd–O4	2.4641(10)	Dy–O4	2.434(4)	Er–O4	2.4106(11)		
Ln–Cl	Gd–Cl1	2.6298(5)	Gd–Cl1	2.6285(4)	Dy–Cl1	2.6087(14)	Er–Cl1	2.5858(4)	Yb–Cl1	2.538(2)
	Gd–Cl1^{i}	2.6298(5)	Gd–Cl2	2.6343(4)	Dy–Cl2	2.5957(14)	Er–Cl2	2.5865(4)	Yb–Cl2	2.507(2)
	Gd–Cl2	2.6527(7)	Gd–Cl3	2.6326(4)	Dy–Cl3	2.5962(14)	Er–Cl3	2.5847(4)	Yb–Cl3	2.529(2)

Table S7. Selected bond angles (°) for complexes $[GdCl_3(thf)_4]$ (**3**), $[GdCl_3(dme)_2]$ (**5**), $[YbCl_3(thf)_3]$ (**8**), $[DyCl_3(dme)_2]$ (**9**) and $[ErCl_3(dme)_2]$ (**10**), with estimated standard deviations in parentheses, with estimated standard deviations in parentheses. Symmetry code: (i) –x+1, –y+1,z

Bond type	$[GdCl_3(thf)_4]$ (**3**)		$[GdCl_3(dme)_2]$ (**5**)		$[DyCl_3(dme)_2]$ (**9**)		$[ErCl_3(dme)_2]$ (**10**)		$[YbCl_3(thf)_3]$ (**8**)	
O–Ln–O	O1^{i}–Gd–O1	70.70(6)	O1–Gd–O2	66.73(4)	O1–Dy–O2	67.51(13)	O1–Er–O2	67.75(4)	O1–Yb–O2	165.3(2)
	O2–Gd–O1	139.36(5)	O1–Gd–O3	157.49(4)	O1–Dy–O3	156.88(13)	O1–Er–O3	156.67(4)		
	O2–Gd–O1^{i}	68.68(5)	O1–Gd–O4	135.94(4)	O1–Dy–O4	136.15(13)	O1–Er–O4	135.94(4)	O1 –Yb–O3	83.5(2)
	O2^{i}–Gd–O1	68.68(5)	O3–Gd–O2	130.34(3)	O3–Dy–O2	130.43(14)	O3–Er–O2	130.38(4)		
	O2^{i}–Gd–O1^{i}	139.36(5)	O4–Gd–O2	72.26(4)	O4–Dy–O2	71.82(14)	O4–Er–O2	71.48(4)	O2 –Yb–O3	82.1(2)
	O2^{i}–Gd–O2	151.96(8)	O4–Gd–O3	66.09(4)	O4–Dy–O3	66.61(13)	O4–Er–O3	67.06(4)		
O–Ln–Cl	O1–Gd–Cl1	87.59(3)	O1–Gd–Cl1	80.27(3)	O1–Dy–Cl1	79.56(10)	O1–Er–Cl1	79.47(3)	O1–Yb–Cl1	88.43(16)
	O1–Gd–Cl1^{i}	86.07(3)	O2–Gd–Cl1	146.67(3)	O2–Dy–Cl1	146.76(10)	O2–Er–Cl1	146.92(3)	O2–Yb–Cl1	89.76(16)
	O1^{i}–Gd–Cl1	86.07(3)	O3–Gd–Cl1	80.54(3)	O3–Dy–Cl1	80.44(10)	O3–Er–Cl1	80.35(3)	O3–Yb–Cl1	87.23(16)
	O1^{i}–Gd–Cl1^{i}	87.60(3)	O4–Gd–Cl1	140.62(3)	O4–Dy–Cl1	140.90(10)	O4–Er–Cl1	141.02(3)	-----	-----
	O1–Gd–Cl2	144.65(3)	O1–Gd–Cl2	89.27(3)	O1–Dy–Cl2	89.45(10)	O1–Er–Cl2	89.61(3)	O1–Yb–Cl2	97.48(18)
	O1^{i}–Gd–Cl2	144.65(3)	O2–Gd–Cl2	78.30(3)	O2–Dy–Cl2	78.54(10)	O2–Er–Cl2	78.69(3)	O2–Yb–Cl2	97.17(18)
	O2–Gd–Cl1	90.82(4)	O3–Gd–Cl2	81.66(3)	O3–Dy–Cl2	81.70(10)	O3–Er–Cl2	81.47(3)	O3–Yb–Cl2	179.21(17)
	O2–Gd–Cl1^{i}	91.06(4)	O4–Gd–Cl2	97.76(3)	O4–Dy–Cl2	98.08(11)	O4–Er–Cl2	98.28(3)	-----	-----
	O2^{i}–Gd–Cl1	91.06(4)	O1–Gd–Cl3	84.90(3)	O1–Dy–Cl3	84.90(10)	O1–Er–Cl3	84.80(3)	O1–Yb–Cl3	89.28(16)
	O2^{i}–Gd–Cl1^{i}	90.82(4)	O2–Gd–Cl3	89.72(3)	O2–Dy–Cl3	89.92(10)	O2–Er–Cl3	90.19(3)	O2–Yb–Cl3	90.69(16)
	O2–Gd–Cl2	75.98(4)	O3–Gd–Cl3	107.41(3)	O3–Dy–Cl3	107.18(10)	O3–Er–Cl3	107.24(3)	O3–Yb–Cl3	85.59(16)
	O2^{i}–Gd–Cl2	75.98(4)	O4–Gd–Cl3	79.39(3)	O4–Dy–Cl3	79.27(11)	O4–Er–Cl3	79.27(3)	-----	-----
Cl–Ln–Cl	Cl1^{i}–Gd–Cl1	172.24(3)	Cl1–Gd–Cl2	97.424(14)	Cl1–Dy–Cl2	97.32(5)	Cl1–Er–Cl2	97.365(12)	Cl1–Yb–Cl2	93.02(9)
	Cl1^{i}–Gd–Cl2	93.882(14)	Cl1–Gd–Cl3	91.966(14)	Cl1–Dy–Cl3	91.63(5)	Cl1–Er–Cl3	91.175(13)	Cl1–Yb–Cl3	172.67(8)
	Cl1–Gd–Cl2	93.882(14)	Cl3–Gd–Cl2	167.972(13)	Cl3–Dy–Cl2	168.39(4)	Cl3–Er–Cl2	168.785(12)	Cl3–Yb–Cl2	94.18(9)

Table S8. Selected bond lengths (Å) for *trans*-[$GdCl_2(thf)_5$]*trans*-[$GdCl_4(thf)_2$] **(4),** *trans*-[$DyCl_2(thf)_5$]*trans*-[$DyCl_4(thf)_2$] **(6),** and *trans*-[$YCl_2(thf)_5$]*trans*-[$YCl_4(thf)_2$] **(7)**, with estimated standard deviations in parentheses

Bond type	*trans*-[$GdCl_2(thf)_5$]*trans*-[$GdCl_4(thf)_2$] **(4)**		[*trans*-[$DyCl_2(thf)_5$]*trans*-[$DyCl_4(thf)_2$] **(6)**		*trans*-[$YCl_2(thf)_5$]*trans*-[$YCl_4(thf)_2$] **(7)**	
$Ln–O_{thf}$	Gd1–O1A	2.407(7)	Dy1–O1	2.388(3)	Y1–O1	2.3753(13)
	Gd1–O1A^{i}	2.407(7)	Dy1–O1^{i}	2.388(3)	Y1–O1^{i}	2.3754(13)
	Gd1–O2	2.401(3)	Dy1–O2	2.379(3)	Y1–O2	2.3649(13)
	Gd1–O2^{i}	2.401(3)	Dy1–O2^{i}	2.379(3)	Y1–O2^{i}	2.3649(13)
	Gd1–O3	2.414(4)	Dy1–O3	2.390(5)	Y1–O3	2.3753(19)
	Gd2–O4	2.360(3)	Dy2–O4	2.338(3)	Y2–O4	2.3151(14)
	Gd2–O4^{ii}	2.360(3)	Dy2–O4^{ii}	2.338(3)	Y2–O4^{ii}	2.3151(14)
M–Cl	Gd1–Cl1	2.6107(9)	Dy1–Cl1	2.5794(11)	Y1–Cl1	2.5750(5)
	Gd1–Cl1^{i}	2.6107(9)	Dy1–Cl1^{i}	2.5794(11)	Y1–Cl1^{i}	2.5750(5)
	Gd2–Cl2	2.6586(9)	Dy2–Cl2	2.6296(12)	Y2–Cl2	2.6235(5)
	Gd2–Cl2^{ii}	2.6567(9)	Dy2–Cl2^{ii}	2.6296(12)	Y2–Cl2^{ii}	2.6236(5)
	Gd2–Cl3	2.6379(10)	Dy2–Cl3	2.6039(11)	Y2–Cl3	2.6019(5)
	Gd2–Cl3^{ii}	2.6379(10)	Dy2–Cl3^{ii}	2.6040(11)	Y2–Cl3^{ii}	2.6019(5)

Symmetry codes: (i) –x+1, y,–z+3/2; (ii) –x+1/2, –y+3/2,–z+2.

Table S9. Selected bond angles (°) for *trans*-[$GdCl_2(thf)_5$]*trans*-[$GdCl_4(thf)_2$] **(4),** *trans*-[$DyCl_2(thf)_5$]*trans*-[$DyCl_4(thf)_2$] **(6),** and *trans*-[$YCl_2(thf)_5$]*trans*-[$YCl_4(thf)_2$] **(7)**, with estimated standard deviations in parentheses

Bond type	*trans*-[$GdCl_2(thf)_5$]*trans*-[$GdCl_4(thf)_2$] **(4)**		[*trans*-[$DyCl_2(thf)_5$]*trans*-[$DyCl_4(thf)_2$] **(6)**		*trans*-[$YCl_2(thf)_5$]*trans*-[$YCl_4(thf)_2$] **(7)**	
O–Ln–O	O1A–Gd1–O1A^{i}	69.7(15)	O1–Dy1–O1^{i}	72.46(15)	O1–Y1–O1^{i}	72.01(7)
	O2–Gd1–O1A	142.3(6)	O2–Dy1–O1	143.74(11)	O2^{i}–Y1–O1	143.51(5)
	O2–Gd1–O1A^{i}	74.0(7)	O2–Dy1–O1^{i}	72.45(11)	O2–Y1–O1	72.69(5)
	O2^{i}–Gd1–O1A	74.0(7)	O2^{i}–Dy1–O1	72.45(11)	O2^{i}–Y1–O1^{i}	72.69(5)
	O2^{i}–Gd1–O1A^{i}	142.3(6)	O2^{i}–Dy1–O1^{i}	143.74(11)	O2–Y1–O1^{i}	143.51(5)
	O2^{i}–Gd1–O2	143.39(13)	O2^{i}–Dy1–O2	143.53(16)	O2^{i}–Y1–O2	143.52(7)
	O2–Gd1–O3	71.70(6)	O2–Dy1–O3	71.77(8)	O2–Y1–O3	71.76(3)
	O2^{i}–Gd1–O3	71.70(6)	O2^{i}–Dy1–O3	71.77(8)	O2^{i}–Y1–O3	71.76(3)
	O3–Gd1–O1A	145.1(7)	O3–Dy1–O1	143.77(7)	O3–Y1–O1	143.99(3)
	O3–Gd1–O1A^{i}	145.1(7)	O3–Dy1–O1^{i}	143.77(7)	O3–Y1–O1	143.99(3)
	O4^{ii}–Gd2–O4	180.0	O4^{ii}–Dy2–O4	180.0	O4^{ii}–Y2–O4	180.0
O–Ln–Cl	O1A–Gd1–Cl1	85.3(5)	O1–Dy1–Cl1	85.86(8)	O1^{i}–Y1–Cl1	85.90(3)
	O1A–Gd1–Cl1^{i}	92.2(5)	O1–Dy1–Cl1^{i}	92.15(8)	O1–Y1–Cl1	92.28(3)
	O1A^{i}–Gd1–Cl1	92.2(5)	O1^{i}–Dy1–Cl1	92.14(8)	O1^{i}–Y1–Cl1^{i}	92.28(3)
	O1A^{i}–Gd1–Cl1^{i}	85.3(5)	O1^{i}–Dy1–Cl1^{i}	85.86(8)	O1–Y1–Cl1^{i}	85.90(3)
	O2–Gd1–Cl1	86.39(7)	O2–Dy1–Cl1	86.57(8)	O2–Y1–Cl1	86.51(3)
	O2–Gd1–Cl1^{i}	94.56(6)	O2–Dy1–Cl1^{i}	94.21(8)	O2–Y1–Cl1^{i}	94.19(3)
	O2^{i}–Gd1–Cl1	94.56(6)	O2^{i}–Dy1–Cl1	94.21(8)	O2^{i}–Y1–Cl1	94.19(3)
	O2^{i}–Gd1–Cl1^{i}	86.39(7)	O2^{i}–Dy1–Cl1^{i}	86.57(8)	O2^{i}–Y1–Cl1^{i}	86.52(3)
	O3–Gd1–Cl1	91.51(2)	O3–Dy1–Cl1	91.23(3)	O3–Y1–Cl1	91.122(12)
	O3–Gd1–Cl1^{i}	91.51(2)	O3–Dy1–Cl1^{i}	91.23(3)	O3–Y1–Cl1^{i}	91.121(13)
	O4–Gd2–Cl2	91.02(7)	O4–Dy2–Cl2	90.94(9)	O4–Y2–Cl2	90.99(4)
	O4–Gd2–Cl2^{ii}	88.98(7)	O4–Dy2–Cl2^{ii}	89.06(9)	O4–Y2–Cl2^{ii}	89.01(4)
	O4^{ii}–Gd2–Cl2	88.98(7)	O4^{ii}–Dy2–Cl2	89.06(9)	O4^{ii}–Y2–Cl2	89.01(4)
	O4^{ii}–Gd2–Cl2^{ii}	91.02(7)	O4^{ii}–Dy2–Cl2^{ii}	90.94(9)	O4^{ii}–Y2–Cl2^{ii}	90.99(4)
	O4–Gd2–Cl3	89.95(7)	O4–Dy2–Cl3	89.98(9)	O4–Y2–Cl3	90.01(4)
	O4–Gd2–Cl3^{ii}	90.05(7)	O4–Dy2–Cl3^{ii}	90.02(9)	O4–Y2–Cl3^{ii}	89.99(4)
	O4^{ii}–Gd2–Cl3	90.06(7)	O4^{ii}–Dy2–Cl3	90.02(9)	O4^{ii}–Y2–Cl3	89.99(4)
	O4^{ii}–Gd2–Cl3^{ii}	89.95(7)	O4^{ii}–Dy2–Cl3^{ii}	89.98(9)	O4^{ii}–Y2–Cl3^{ii}	90.01(4)
Cl–Ln–Cl	Cl1–Gd1–Cl1^{i}	176.98(5)	Cl1–Dy1–Cl1^{i}	177.53(6)	Cl1–Y1–Cl1^{i}	177.76(3)
	Cl2–Gd2–Cl2^{ii}	180.00(4)	Cl2–Dy2–Cl2^{ii}	180.0	Cl2–Y2–Cl2^{ii}	180.0
	Cl3–Gd2–Cl3^{ii}	180.0	Cl3–Dy2–Cl3^{ii}	180.0	Cl3–Y2–Cl3^{ii}	180.0
	Cl3−Gd2–Cl2	92.22(3)	Cl3–Dy2–Cl2	92.20(4)	Cl3–Y2−Cl2	92.170(15)
	Cl3−Gd2–Cl2^{ii}	87.78(3)	Cl3–Dy2–Cl2^{ii}	87.80(4)	Cl3–Y2–Cl2^{ii}	87.830(16)
	Cl3^{ii}–Gd2–Cl2	87.78(3)	Cl3^{ii}–Dy2–Cl2	87.81(4)	Cl3^{ii}–Y2–Cl2	87.830(15)
	Cl3^{ii}–Gd2–Cl2^{ii}	92.22(3)	Cl3^{ii}–Dy2–Cl2^{ii}	92.20(4)	Cl3^{ii}–Y2–Cl2^{ii}	92.171(15)

Symmetry code: (i) –x+1, y,–z+3/2; (ii) –x+1/2, –y+3/2,–z+2.

Table S10. Selected dimensions (bond distances and angles) about the metal ions in complex **11.** Bond lengths are in Angstroms (Å) and angles in degrees (°). Standard deviations are in parentheses

Bond lengths / Å			
Gd1–O2	2.377(3)	Gd2–Cl4	2.7336(11)
Gd1–O3	2.394(3)	Gd2–Cl3	2.7558(11)
Gd1–O1	2.421(3)	Gd2–Cl6	2.7562(11)
Gd1–Cl1	2.5615(13)	Gd2–C7	2.917(5)
Gd1–Cl2	2.7406(11)	Gd3–O7	2.380(3)
Gd1–Cl8^{i}	2.7447(11)	Gd3–O8	2.398(3)
Gd1–Cl3	2.7528(12)	Gd3–O6	2.418(3)
Gd2–O4	2.363(3)	Gd3–Cl7	2.5596(13)
Gd2–O5	2.448(3)	Gd3–Cl8	2.7351(11)
Gd2–O3	2.507(3)	Gd3–Cl2^{ii}	2.7577(11)
Gd2–O6	2.518(3)	Gd3–Cl6	2.7664(12)
Gd2–Cl5	2.7109(11)		
Angles / °			
O2–Gd1–O3	69.87(11)	O6–Gd2–Cl3	119.59(7)
O2–Gd1–O1	137.31(11)	Cl5–Gd2–Cl3	84.04(3)
O3–Gd1–O1	68.69(11)	Cl4–Gd2–Cl3	98.16(3)
O2–Gd1–Cl1	86.54(10)	O4–Gd2–Cl6	96.23(9)
O3–Gd1–Cl1	98.10(8)	O5–Gd2–Cl6	77.10(8)
O1–Gd1–Cl1	89.47(9)	O3–Gd2–Cl6	120.79(7)
O2–Gd1–Cl2	146.03(9)	O6–Gd2–Cl6	70.41(7)
O3–Gd1–Cl2	138.00(8)	Cl5–Gd2–Cl6	96.68(3)
O1–Gd1–Cl2	75.92(8)	Cl4–Gd2–Cl6	86.79(3)
Cl1–Gd1–Cl2	103.58(4)	Cl3–Gd2–Cl6	169.60(4)
O2–Gd1–Cl8^{i}	73.97(9)	O4–Gd2–C7	144.39(12)
O3–Gd1–Cl8^{i}	140.62(8)	O5–Gd2–C7	149.68(12)
O1–Gd1–Cl8^{i}	148.70(8)	O3–Gd2–C7	25.53(11)
Cl1–Gd1–Cl8^{i}	94.72(4)	O6–Gd2–C7	25.43(11)
Cl2–Gd1–Cl8^{i}	72.94(3)	Cl5–Gd2–C7	73.96(9)
O2–Gd1–Cl3	85.34(9)	Cl4–Gd2–C7	73.77(9)
O3–Gd1–Cl3	71.12(8)	Cl3–Gd2–C7	94.51(9)
O1–Gd1–Cl3	90.76(9)	Cl6–Gd2–C7	95.65(9)
Cl1–Gd1–Cl3	168.27(4)	O7–Gd3–O8	140.66(12)
Cl2–Gd1–Cl3	87.84(4)	O7–Gd3–O6	70.96(11)
Cl8^{i}–Gd1–Cl3	91.16(4)	O8–Gd3–O6	69.70(11)
O4–Gd2–O5	65.90(12)	O7–Gd3–Cl7	86.93(10)
O4–Gd2–O3	127.84(11)	O8–Gd3–Cl7	94.26(10)
O5–Gd2–O3	150.79(10)	O6–Gd3–Cl7	90.77(8)
O4–Gd2–O6	147.45(11)	O7–Gd3–Cl8	145.24(9)
O5–Gd2–O6	134.09(10)	O8–Gd3–Cl8	74.10(9)
O3–Gd2–O6	50.94(9)	O6–Gd3–Cl8	143.76(8)
O4–Gd2–Cl5	137.26(9)	Cl7–Gd3–Cl8	90.16(4)
O5–Gd2–Cl5	77.67(8)	O7–Gd3–Cl2^{ii}	74.19(9)
O3–Gd2–Cl5	77.38(7)	O8–Gd3–Cl2^{ii}	142.36(10)
O6–Gd2–Cl5	74.94(7)	O6–Gd3–Cl2^{ii}	141.53(8)
O4–Gd2–Cl4	73.54(9)	Cl7–Gd3–Cl2^{ii}	103.25(4)
O5–Gd2–Cl4	133.94(8)	Cl8–Gd3–Cl2^{ii}	72.82(3)
O3–Gd2–Cl4	73.42(7)	O7–Gd3–Cl6	85.40(10)
O6–Gd2–Cl4	76.13(7)	O8–Gd3–Cl6	81.77(10)
Cl5–Gd2–Cl4	147.73(4)	O6–Gd3–Cl6	71.63(8)
O4–Gd2–Cl3	76.60(9)	Cl7–Gd3–Cl6	162.29(4)
O5–Gd2–Cl3	92.98(8)	Cl8–Gd3–Cl6	105.16(4)
O3–Gd2–Cl3	69.53(7)	Cl2^{ii}–Gd3–Cl6	89.98(4)

Symmetry code: (i) x+1,y,z; (ii) x–1,y,z.

Table S11. Selected distances (Å) and angles (°) about the gadolinium ions in the tetranuclear $[Ln_4(O_2)_2Cl_8(thf)_{10}]\cdot 3thf$ (**12**). Standard deviations are in parentheses

Bond lengths / Å			
Gd1−O1	2.474(2)	Gd2−O4	2.402(2)
Gd1−O2	2.486(2)	Gd2−O3	2.421(2)
Gd1−O8	2.3376(19)	Gd2−O9^{i}	2.367(2)
Gd1−O9	2.345(2)	Gd2−O9	2.384(2)
Gd1−Cl1	2.6604(7)	Gd2−O5	2.513(2)
Gd1−Cl3	2.6732(7)	Gd2−Cl4	2.8130(7)
Gd1−Cl4	2.8076(7)	Gd2−Cl2^{i}	2.8419(7)
Gd1−Cl2	2.8432(7)	Gd2−Gd2^{i}	3.5682(4)
Gd1−Gd2	3.9874(3)	O8−O9	1.526(3)
Gd1−Gd2^{i}	4.0018(4)	Gd2···Gd2^{i}	3.5680(5)
Gd2−O8^{i}	2.364(2)	Gd2···Gd1	3.9874(5)
Gd2−O8	2.365(2)	Gd1···Gd2^{i}	4.0016(7)
Angles / °			
O8−Gd1−O9	38.04(6)	O2−Gd1−Cl4	73.02(5)
O8−Gd1−O1	140.63(7)	Cl1−Gd1−Cl4	91.45(2)
O9−Gd1−O1	139.34(7)	Cl3−Gd1−Cl4	93.33(2)
O8−Gd1−O2	138.71(7)	O8−Gd1−Cl2	72.33(5)
O9−Gd1−O2	142.09(7)	O9−Gd1−Cl2	72.59(5)
O1−Gd1−O2	71.31(7)	O1−Gd1−Cl2	72.72(5)
O8−Gd1−Cl1	120.01(5)	O2−Gd1−Cl2	143.73(5)
O9−Gd1−Cl1	81.99(5)	Cl1−Gd1−Cl2	95.22(2)
O1−Gd1−Cl1	80.70(5)	Cl3−Gd1−Cl2	92.44(2)
O2−Gd1−Cl1	83.50(5)	Cl4−Gd1−Cl2	143.15(2)
O8−Gd1−Cl3	79.76(5)	O8−Gd1−Gd2	32.22(5)
O9−Gd1−Cl3	117.79(5)	O9−Gd1−Gd2	32.82(5)
O1−Gd1−Cl3	84.18(5)	O1−Gd1−Gd2	170.97(5)
O2−Gd1−Cl3	79.54(5)	O2−Gd1−Gd2	117.72(5)
Cl1−Gd1−Cl3	160.17(2)	Cl1−Gd1−Gd2	99.630(17)
O8−Gd1−Cl4	72.98(5)	Cl3−Gd1−Gd2	97.316(18)
O9−Gd1−Cl4	72.56(5)	Cl4−Gd1−Gd2	44.867(15)
O1−Gd1−Cl4	144.09(5)	Cl2−Gd1−Gd2	98.296(16)
O8−Gd1−Gd2^{i}	31.87(5)	O3−Gd2−Cl4	85.30(5)
O9−Gd1−Gd2^{i}	32.03(5)	O5−Gd2−Cl4	71.21(5)
O1−Gd1−Gd2^{i}	117.94(5)	O8^{i}−Gd2−Cl2^{i}	72.01(5)
O2−Gd1−Gd2^{i}	170.23(5)	O8−Gd2−Cl2^{i}	142.04(5)
Cl1−Gd1−Gd2^{i}	100.638(18)	O9^{i}−Gd2−Cl2^{i}	72.32(5)
Cl3−Gd1−Gd2^{i}	97.748(18)	O9−Gd2−Cl2^{i}	141.02(5)
Cl4−Gd1−Gd2^{i}	97.909(15)	O4−Gd2−Cl2^{i}	86.92(5)
Cl2−Gd1−Gd2^{i}	45.245(14)	O3−Gd2−Cl2^{i}	85.47(5)

Gd2−Gd1−Gd2^{i}	53.055(6)	O5−Gd2−Cl2^{i}	71.92(5)
O8^{i}−Gd2−O8	82.03(7)	Cl4−Gd2−Cl2^{i}	143.00(2)
O8^{i}−Gd2−O9^{i}	37.63(6)	O8^{i}−Gd2−Gd2^{i}	41.02(5)
O8−Gd2−O9^{i}	70.22(7)	O8−Gd2−Gd2^{i}	41.01(5)
O8^{i}−Gd2−O9	69.95(7)	O9^{i}−Gd2−Gd2^{i}	41.50(5)
O8−Gd2−O9	37.48(6)	O9−Gd2−Gd2^{i}	41.14(5)
O9^{i}−Gd2−O9	82.64(7)	O4−Gd2−Gd2^{i}	101.42(5)
O8^{i}−Gd2−O4	117.29(7)	O3−Gd2−Gd2^{i}	101.92(5)
O8−Gd2−O4	80.82(7)	O5−Gd2−Gd2^{i}	178.00(5)
O9^{i}−Gd2−O4	79.93(7)	Cl4−Gd2−Gd2^{i}	108.423(16)
O9−Gd2−O4	118.03(7)	Cl2^{i}−Gd2−Gd2^{i}	108.532(16)
O8^{i}−Gd2−O3	81.07(7)	O8^{i}−Gd2−Gd1	100.42(5)
O8−Gd2−O3	117.82(7)	O8−Gd2−Gd1	31.80(5)
O9^{i}−Gd2−O3	118.34(7)	O9^{i}−Gd2−Gd1	100.58(5)
O9−Gd2−O3	80.67(7)	O9−Gd2−Gd1	32.21(5)
O4−Gd2−O3	156.66(7)	O4−Gd2−Gd1	95.14(5)
O8^{i}−Gd2−O5	140.26(7)	O3−Gd2−Gd1	95.38(5)
O8−Gd2−O5	137.67(7)	O5−Gd2−Gd1	115.89(5)
O9^{i}−Gd2−O5	137.86(7)	Cl4−Gd2−Gd1	44.758(15)
O9−Gd2−O5	139.43(7)	Cl2^{i}−Gd2−Gd1	172.186(15)
O4−Gd2−O5	76.63(7)	Gd2^{i}−Gd2−Gd1	63.680(7)
O3−Gd2−O5	80.03(7)	O8^{i}−Gd2−Gd1^{i}	31.47(5)
O8^{i}−Gd2−Cl4	141.05(5)	O8−Gd2−Gd1^{i}	100.02(5)
O8−Gd2−Cl4	72.50(5)	O9^{i}−Gd2−Gd1^{i}	31.70(5)
O9^{i}−Gd2−Cl4	142.08(5)	O9−Gd2−Gd1^{i}	99.88(5)
O9−Gd2−Cl4	71.92(5)	O4−Gd2−Gd1^{i}	95.01(5)
O4−Gd2−Cl4	87.61(5)	O3−Gd2−Gd1^{i}	95.21(5)
O5−Gd2−Gd1^{i}	117.13(5)	Gd1−O8−Gd2^{i}	116.67(8)
Cl4−Gd2−Gd1^{i}	171.618(15)	Gd1−O8−Gd2	115.98(8)
Cl2^{i}−Gd2−Gd1^{i}	45.272(15)	Gd2^{i}−O8−Gd2	97.97(7)
Gd2^{i}−Gd2−Gd1^{i}	63.265(6)	Gd1−O9−Gd2^{i}	116.27(8)
Gd1−Gd2−Gd1^{i}	126.945(6)	Gd1−O9−Gd2	114.97(8)
Gd2^{i}−Cl2−Gd1	89.48(2)	Gd2^{i}−O9−Gd2	97.36(7)
Gd1−Cl4−Gd2	90.38(2)		

Symmetry code: (i) −x+1, −y+1, −z+1.

Table S12. Weak intra and intermolecular C−H···Cl contacts in the unit cell of the tetranuclear **12,** $[\{(thf)_2Cl_2Gd(\mu-Cl)_2(\mu_3-O_2)Gd(thf)_3\}_2]\cdot 3thf$. Distances in Ångstroms and angles in degrees

Type	D-H···A	d(D-H)	d(H···A)	d(D···A)	<(DHA)
Intramolecular	C4−H4B−Cl3	0.99	2.78	3.445(4)	124.7
Intramolecular	C7−H7A−O6	0.99	2.61	3.570(6)	163.7
Intramolecular	C9−H9B−Cl1	0.99	2.78	3.711(4)	156.8
Intermolecular	C10−H10B−Cl1^{ii}	0.99	2.78	3.628(4)	144.5
Intermolecular	C12−H12A−Cl3^{i}	0.99	2.70	3.650(4)	160.4
Intramolecular	C13−H13A−Cl3	0.99	2.83	3.813(4)	171.7
Intermolecular	C15−H15B−Cl1^{iii}	0.99	2.83	3.604(4)	135.3
Intermolecular	C24−H24A−Cl4	0.99	2.81	3.684(4)	147.4

Symmetry codes: (i) 1–x, 1–y, 1–z ; (ii) 1–x, –y, 1–z ; (iii) x, 1+y, z

Table S13. ^{1}H (400.13 MHz) and ^{13}C (100.03 MHz) NMR analysis of the volatiles collected from the reaction mixture(*) that produced the polynuclear complex **11**

Molecule / Assignment (**)	Chemical shift, ^{1}H, ppm	Multiplicity	Coupling constant, Hz	Chemical shift, $^{13}C\{^1H\}$, ppm
Teof, $-CH_3$	1.23	t	7.1	15.0
Teof, $-CH_2$	3.60	q	7.1	59.5
Teof, −CH	5.17	s	-----	112.4
Ethanol, $-CH_3$	1.24	t	7.0	18.4
Ethanol, $-CH_2$	3.71	q	7.0	58.4
Ethyl formate, $-CH_3$	1.31	td	7.2; 0.6	14.2
Ethyl formate, $-CH_2$	4.23	qd	7.2; 0.8	60.0
Ethyl formate, −CH	8.04	tq	0.8; 0.6	161.1
Isopropanol, $-CH_3$	1.205	d	6.1	25.4
Isopropanol, −CH	4.02	hep	6.1	64.4
Diethyl-isopropyl-orthoformate, $-OCH_2\mathbf{CH_3}$	1.23	t	7.1	15.0
Diethyl-isopropyl-orthoformate, $-O\mathbf{CH_2}CH_3$	3.61	q	7.1	59.1
Diethyl-isopropyl-orthoformate, $-OCH(\mathbf{CH_3})_2$	1.204	d	6.2	21.8
Diethyl-isopropyl-orthoformate, $-O\mathbf{CH}(CH_3)_2$	3.99	hep	6.2	67.8
Isopropyl formate, $-OCH(\mathbf{CH_3})_2$	1.28	dd	6.2; 0.5	22.7
Isopropyl formate, $-O\mathbf{CH}(CH_3)_2$	5.13	dhep	6.2; 0.8	67.2
Isopropyl formate, −OC(O)**H**	8.00	dhep	0.8; 0.5	168.0
Water (from $CDCl_3$)	1.57	s	-----	-----

(*) The volatiles were collected by vacuum pumping and condensation in liquid N_2 when the reaction mixture was dried to give Product **A** (see Experimental in the main text).

(**) Assignments based on ^{1}H, $^{13}C\{^1H\}$ and DEPT NMR data.

Table S14. Continuous shape measures of coordination polyhedra for complexes $[Gd_2Cl_4(\mu\text{-}Cl)_2(Pr^iOH)_6]$ **(1)**, $[\{GdCl(\mu\text{-}Cl)_2(thf)_2\}_\infty]$ **(2)**, $[DyCl_3(dme)_2]$ **(9)**, and $[\{Gd_3Cl_3(\mu\text{-}Cl)_4(\mu\text{-}H_3CCOO)(C_3H_8O_2)(Pr^iOH)_4]\cdot Pr^iOH\}_\infty]$ **(11)**, obtained with the SHAPE 2.1 software[21]

	Geometry	Gd1	Gd2
$[Gd_2Cl_4(\mu\text{–}Cl)_2(Pr^iOH)_6]$ **(1)**	Heptagon (D_{7h})	35.216	35.019
	Hexagonal pyramid (C_{6v})	20.257	20.613
	Pentagonal bipyramid (D_{5h})	6.691	7.727
	Capped octahedron (C_{3v})	**0.720**	**0.464**
	Capped trigonal prism (C_{2v})	1.365	2.215
	Johnson pentagonal bipyramid J13 (D_{5h})	11.395	10.962
	Johnson elongated triangular pyramid J7 (C_{3v})	21.234	21.653

	Geometry	Gd1
$[\{GdCl(\mu\text{–}Cl)_2(thf)_2\}_\infty]$ **(2)**	Heptagon (D_{7h})	34.771
	Hexagonal pyramid (C_{6v})	23.417
	Pentagonal bipyramid (D_{5h})	**1.498**
	Capped octahedron (C_{3v})	4.945
	Capped trigonal prism (C_{2v})	3.710
	Johnson pentagonal bipyramid J13 (D_{5h})	3.871
	Johnson elongated triangular pyramid J7 (C_{3v})	20.437

	Geometry	Gd1
$[DyCl_3(dme)_2]$ **(9)**	Heptagon (D_{7h})	34.611
	Hexagonal pyramid (C_{6v})	22.792
	Pentagonal bipyramid (D_{5h})	**1.881**
	Capped octahedron (C_{3v})	4.539
	Capped trigonal prism (C_{2v})	2.946
	Johnson pentagonal bipyramid J13 (D_{5h})	6.366
	Johnson elongated triangular pyramid J7 (C_{3v})	21.328

(Continues on the next page)

Table S14. Continuation

	Geometry	Gd1	Gd3
[{$Gd_3Cl_3(\mu–Cl)_4(\mu–H_3CCOO)$-$(C_3H_8O_2)(Pr^iOH)_4]\cdot Pr^iOH\}_\infty$] **(11)**	Heptagon (D_{7h})	34.949	32.893
	Hexagonal pyramid (C_{6v})	24.578	22.860
	Pentagonal bipyramid (D_{5h})	**1.402**	**1.762**
	Capped octahedron (C_{3v})	6.251	5.226
	Capped trigonal prism (C_{2v})	5.183	3.742
	Johnson pentagonal bipyramid J13 (D_{5h})	5.796	5.987
	Johnson elongated triangular pyramid J7 (C_{3v})	22.632	22.379
	Geometry	**Gd2**	
	Octagon (D_{8h})	32.981	
	Heptagonal pyramid (C_{7v})	24.625	
	Hexagonal bipyramid (D_{6h})	9.980	
	Cube (O_h)	7.499	
	Square antiprism (D_{4d})	4.110	
	Triangular dodecahedron (D_{2d})	4.015	
	Johnson gyrobifastigium J26 (D_{2d})	11.320	
	Johnson elongated triangular bipyramid J14 (D_{3h})	27.662	
	Biaugmented trigonal prism J50 (C_{2v})	5.091	
	Biaugmented trigonal prism (C_{2v})	**3.871**	
	Snub diphenoid J84 (D_{2d})	6.433	
	Triakis tetrahedron (T_d)	8.293	
	Elongated trigonal bipyramid (D_{3h})	23.543	

Table S15. Best fitting parameters (Equation 2) of the isothermal frequency dependence of the $\chi''(\nu)$ plots reported in Figure 4 (main text) for product **9**, under an applied field of 1 kOe

$\chi''(\nu)$ Component / Parameter	$\tau_{0\ Orbach}$ (s)	U_{eff} (cm^{-1})	$\tau_{0,\ Raman}$ (s)	w_{eff} (cm^{-1})	R^2
Low-frequency peaks	$1.47(7)\cdot10^{-10}$	139 (fixed)	$4(1)\cdot10^{-8}$	46.8(2)	0.9995
High-frequency peaks	$5.2(1)\cdot10^{-11}$	36(7)	-----	-----	0.8783

Table S16. Energy splitting of the first eight Kramers doublets for product **9**

Kramers doublet	Energy (cm^{-1})
1	0
2	139.73
3	189.58
4	266.65
5	299.65
6	322.63
7	362.50
8	401.74

Table S17. Calculated *g*-tensors of the ground and first excited Kramers doublets for **9**

	g_x	g_y	g_z
Doublet 1	0.037707	0.069263	19.852573
Doublet 2	1.464784	2.961423	16.586063

REFERENCES

1. E. H. Cordes and H. G. Bull, *Chem. Rev.*, 1974, **74**, 581-603.
2. G. R. Willey, T. J. Woodman and M. G. B. Drew, *Polyhedron*, 1997, **16**, 3385-3393.
3. R. E. Marsh, *CCDC 237353: Experimental Crystal Structure Determination*, 2004, DOI: 10.5517/cc7yzkp, WebCSD, Cambridge, UK.
4. R. Marsh, *Acta Crystallogr., Sect. B*, 2004, **60**, 252-253.
5. D. B. Dell'Amico, F. Calderazzo, C. della Porta, A. Merigo, P. Biagini, G. Lugli and T. Wagner, *Inorg. Chim. Acta*, 1995, **240**, 1-3.
6. G. Wei, H. Gao, Z. Jin and Q. Shen, *CCDC 1279470: Experimental Crystal Structure Determination*, https://www.ccdc.cam.ac.uk/structures/Search?Ccdcid=1279470&DatabaseToSearch=Published, 1990, WebCSD, Cambridge, UK.
7. G. B. Deacon, T. Feng, P. C. Junk, B. W. Skelton, A. N. Sobolev and A. H. White, *Aust. J. Chem.*, 1998, **51**, 75-89.
8. S. Anfang, K. Dehnicke and J. Magull, *Z. Naturforsch. B*, 1996, **51**, 531-535.
9. G. B. Deacon, T. Feng, P. C. Junk, G. Meyer, N. M. Scott, B. W. Skelton and A. H. White, *Aust. J. Chem.*, 2001, **53**, 853-865.
10. T. Lis and J. Utko, *CCDC 2052291: Experimental Crystal Structure Determination*, 2020, DOI: 10.5517/ccdc.csd.cc26wkym, WebCSD, Cambridge, UK.
11. G. R. Willey, P. R. Meehan, T. J. Woodman and M. G. B. Drew, *Polyhedron*, 1997, **16**, 623-627.
12. P. Sobota, J. Utko and S. Szafert, *Inorg. Chem.*, 1994, **33**, 5203-5206.
13. A. A. Coelho, *J. Appl. Crystallogr.*, 2018, **51**, 210-218.
14. G. B. Deacon, T. D. Tuong, D. L. Wilkinson and T. Marks, in *Inorg. Synth.*, 1990, DOI: https://doi.org/10.1002/9780470132593.ch72, pp. 286-291.
15. K. Nakamoto, *Infrared and Raman Spectra of Inorganic and Coordination Compounds Part B*, New Jersey, 6th edn., 1996.
16. U. Baisch, D. B. DellAmico, F. Calderazzo, R. Conti, L. Labella, F. Marchetti and E. A. Quadrelli, *Inorg. Chim. Acta*, 2004, **357**, 1538-1548.
17. R. M. Silverstein, F. X. Webster, D. J. Kiemle and D. L. Bryce, *Spectrometric Identification of Organic Compounds*, Wiley, New York, 8th edn., 2014.
18. F. B. R. D. Iorio, A. M. A. Liberatore, I. H. J. Koh, C. Otani and F. F. Camilo, *Ozone: Sci. Eng.*, 2016, **38**, 253-260.
19. K. Ito and H. J. Bernstein, *Can. J. Chem.*, 1956, **34**, 170-178.
20. V. Vacque, B. Sombret, J. P. Huvenne, P. Legrand and S. Suc, *Spectrochim. Acta A Mol. Biomol. Spectrosc.*, 1997, **53**, 55-66.
21. M. Llunell, D. Casanova, J. Cirera, J. Bofill, P. Alemany, S. Alvarez, M. Pinsky and D. Avnir, *Program for the Stereochemical Analysis of Molecular Fragments by Means of Continuous Shape Measures and Associated Tools*, University of Barcelona, Barcelona, Spain, 2005.